universität wien

DIPLOMARBEIT / DIPLOMA THESIS

Titel der Diplomarbeit / Title of the Diploma Thesis

„Biophysical characterization of nucleic acid based polyplexes and auropolyplexes“

verfasst von / submitted by

Marko Zrilic

angestrebter akademischer Grad / in partial fulfilment of the requirements for the degree of

Magister der Pharmazie (Mag.pharm.)

Wien, 2019 / Vienna, 2019

Studienkennzahl lt. Studienblatt / degree programme code as it appears on the student record sheet:	A 449
Studienrichtung lt. Studienblatt / degree programme as it appears on the student record sheet:	Diplomstudium Pharmazie
Betreut von / Supervisor:	Univ.-Prof. Dipl.-Ing. Dr. Manfred Ogris
Mitbetreut von / Co-Supervisor	Dr. Haider Sami

Acknowledgment

It is a genuine pleasure to express my deep sense of thanks and gratitude to my professor and supervisor Univ.-Prof. Dipl.-Ing. Dr. Manfred Ogris giving me the opportunity to carry out a diploma thesis in his research team at the University of Vienna.

I would like to extend my sincere gratitude to Dr. Haider Sami supporting all the way with exceptional kindness and ability to share an amazing amount of knowledge. Additional, his keen interest and encouragement were a tremendous help. Without him, this work would not be possible.

I am also very grateful to all friends and members of my family especially my sister Sara and my girlfriend Sanja for providing love and care during studies and forever.

Last but not least I am deeply thankful and blessed for my greatest inspiration, the woman with extraordinary skill to bring out the best in me, to my mother Violeta.

1.Table of contents

Contents

2. Abstract

Gold nanoparticles and linear polyethyleneimine [LPEI] are commonly used nonviral gene delivery vectors and have been extensively studied. They are promising tools for both gene delivery and gene therapy. Combined with nucleic acids, they create so-called polyplexes or auropolyplexes focusing on optimal delivery efficiency.

This thesis focused on these imaging suitable macromolecular vectors. Namely, biophysical characterization was conducted aiming at reproducibility in production along with the quantification of LPEI payload on nanoparticles. Firstly, we modified gold nanoparticles using LPEI coating. To test further whether the coating phase was successful, SPR (surface plasmon resonance) shifts were compared and finally, complexation with SSO (splice switching oligonucleotides) was conducted. Using gel retardation the complexation within particles was visualized and analyzed. After observing the process of coating, we next sought to calculate the total LPEI used for it and reveal the reproducibility of measurements. Therefore, two approaches were employed: indirect quantification [evaluation of LPEI leftovers in supernatant and washes] and direct quantification [evaluation of LPEI directly on coated gold nanoparticles] using Copper assay as a standard method. Moreover, from the beginning and at each step validation of particle size [by nanoparticle tracking analysis] was needed as well as monitoring their UV-Vis spectroscopy profile in order to establish correlations between SPR shift and complexation and also for observing aggregation tendency.

Furthermore, as the second part of the thesis, we studied complexation of siRNA by PEI of different topologies [LPEI and BPEI] to compare the nucleic acid condensation by gel retardation assays.

3. Abstract

Gold basierende Nanopartikeln und lineares Polyethylenimin [LPEI] sind geeignete nicht-viralen Vektoren für den Transfer von Nukleinsäuren in Zielzellen und stellen ein geeignetes Instrument für gentherapeutische Ansätze dar. In Verbindung mit Nukleinsäuren bilden sie sogenannte Polyplexe oder Auropolyplexe, die auf die optimale Lieferungseffektivität fokussiert sind. Diese Diplomarbeit beschäftigt sich mit der biophysikalischen Charakterisierung dieser auch für bildgebende Verfahren geeigneter makromolekularer Vektoren. Verschiedene biophysikalische Methoden zur Charakterisierung wurden angewendet, mit dem Ziel die Reproduzierbarkeit der Partikelherstellung zu verbessern und die Menge an Gold-gebundenen LPEI (coating) zu bestimmen. Zuerst wurden Gold-Nanopartikel mittels LPEI coating modifiziert. Um zu überprüfen, ob das coating erfolgreich durchgeführt wurde, wurden SPR (surface plasmon resonance) shifts verglichen und schließlich eine Komplexierung mit SSO (splice switching oligonucleotides) durchgeführt. Mittels eines Gelretadierungsassays wurde die Komplexierung von SSO visualisiert und analysiert. Nach dem abgeschlossenen Coating-Prozess wurde die Gesamtmenge LPEI, die zum Coating verwendet wurde, berechnet. Dies gab Aufschluss über die Reproduzierbarkeit der Messungen. Es wurden zwei verschiedene Ansätze evaluiert: zum einen die indirekte Quantifizierung [Quantifizierung von LPEI im Reaktionsüberstand und in den Waschlösungen] und zum anderen die direkte Quantifizierung [Quantifizierung von LPEI auf den beschichteten Gold-Nanopartikeln]. Dazu wurde ein in etablierter Assay auf Basis von Kupferionen eingesetzt. Während des gesamten Prozesses wurde die Partikelgröße mittels Nanopartikel Tracking Analyse bestimmt. Zudem wurden UV-Vis Spektroskopie Profile erstellt, um etwaige Korrelationen zwischen SPR shift und Komplexierung herzustellen. Zusätzlich wurde während des Prozesses beobachtet, ob es eine Tendenz zur Aggregation gibt.

In einem weiteren Projekt wurden versucht, das molare Verhältnis von Nukleinsäure (siRNA) und PEI [LPEI und BPEI] zu optimieren.

4. List of Abbreviations

AL	Coated gold nanoparticles [**A**u+**L**PEI]
ASO	Antisense oligonucleotides
Au	Gold
BPEI	Branched polyethyleneimine
DLS	Dynamic Light Scattering
dsRNA	Double strand RNA
EtBr	Ethidium Bromide
HBS	HEPES buffered saline
LPEI	Linear polyethyleneimine
MMCT	Center for Macromolecular Cancer Therapy
MQ/MQ-water	Ultrapure water
NP(s)	Nanoparticle(s)
N/P	Nitrogen/phosphate [groups ratio]
NTA	Nanoparticle Tracking Analysis
pDNA	Plasmid DNA
PEG	Polyethylene glycol
PEI	Polyethyleneimine
PPX(s)	Polyplex(es)
PS	Phosphorothioate
RISC	RNA induced silencing complex
SD	Standard deviation
SB	Sodium Borate [buffer]
siRNA	Small interfering RNA
SOP	Standard Operating Protocol
SPR	Surface plasmon resonance
SSO	Splice switching oligonucleotides

5. Introduction

5.1 Nucleic acid therapy

When it comes to diseases that are not able to be treated with convention therapeutic strategies, gene therapy reaches the central stage of medicine (Yokoo *et al.*, 2018). Since the first human gene therapy conducted on humans at the NIH clinical center (Blaese *et al.*, 1995), numerous trials have been carried out until now. Most trials (75%) were based on viral-vector as a delivery tool. Despite the fact that this approach granted a high gene expression for a long period, there have been lethal cases of as carcinogenesis noted (S. Hacein-Bey-Abina *et al.*, 2003; Salima Hacein-Bey-Abina *et al.*, 2003; Howe *et al.*, 2008). All this resulted in an increased focus on nonviral vector-based delivery methods, characterized as being biologically safer with less antigenicity (Yokoo *et al.*, 2018). Among many other obstacles like ethical concerns, lack of long term efficacy, production costs, off-targeting effects and toxicity, endosomal-trapping, intracellular uptake, etc., key challenge and a major concern still remain critical and that is delivery of nucleic acid to the site of action (Sridharan and Gogtay, 2016). This gene transfer was once described as 'the Achilles heel' of gene therapy (Somia and Verma, 2000).

Although the potential of nucleic acids as a stand-alone therapeutic has been recognized as promising for more than 40 years, this approach has recently gained immense therapeutic potential (Sridharan and Gogtay, 2016). Thus far, the majority of clinical trials addressed the oncology field and monogenetic diseases followed by infectious and cardiovascular diseases (Ginn *et al.*, 2018). The progress has been slow and only a few gene therapies are approved for humans up to date. Nevertheless, none of these would be possible without technological advances in biology and the engagement of scientists worldwide. Along with this improved understanding of the molecular basis of diseases, there is no doubt that nucleic acid-based therapies will soon or later be an established reality and part of the standard cure in a wide spectrum of diseases.

5.2 siRNA based nucleic acid therapy

In the early 1980s, it has been discovered that RNAs are responsible not only for the transfer of information between DNA and protein synthesis but for many other genome functions at some of the most important levels. After this, it was difficult to overestimate the role of RNA. Then in 1998, RNA interference [RNAi] has been used for the first time in the nematode *Caenorhabditis elegans* to manipulate gene expression (Fire *et al.*, 1998).

RNA interference serves as a powerful defense mechanism, protecting genome integrity against the invasion of mobile genetic materials such as viruses, transgenes, transposons and probably many others. This regulatory mechanism is a fundamental pathway in a broad range of eukaryotic species acting generally inhibitory in both somatic and germline cells (Carthew and Sontheimer, 2009).

Short interfering RNAs or siRNA are characterized by the double-stranded nature of their precursors [dsRNA]. They are 21-23 nucleotides long and they play a leading role in the post-transcriptional gene silencing process. Generally, siRNAs can be synthesized chemically and then transfected into the cell. Also, they are more stable compared to DNA oligonucleotides and basically, the whole process occurs in the cytoplasm which makes things even more uncomplicated. Subsequently, siRNA associates with RISC [RNA induced silencing complex], binds complementary mRNAs and finally results in their degradation (Sridharan and Gogtay, 2016).

5.3 Splice switching oligo based nucleic acid therapy

Mutations that can cause disruption in the process of pre-mRNA splicing are the underlying origin of many genetic diseases. Besides RNA interference, antisense oligonucleotides [ASO] offer great potential for RNA-targeting and splicing modifications that are not possible with other antisense techniques or siRNA. These are two strategies that are most commonly used for gene knockdown and becoming a routine tool for laboratory research (Watts and Corey, 2012).

SSOs or splice switching oligonucleotides are ASOs that are comprised of 15 to 30 nucleotides and synthetically produced. Those antisense modified nucleic acids are designed to bind a complementary pre-mRNA through Watson-Crick base-pairing, creating a steric block which prevents attaching of splicing factors and thus manipulates normal protein production. As well as inhibition, SSOs can also be used to activate or enhance splicing at a particular site [Figure 1]. In comparison to siRNA, the primary aim of SSO therapy is to alter splicing and not to induce degradation of pre-mRNA. Currently, nearly all of the splice-switching ASOs trials are focused on the treatment of Duchenne- and spinal muscular dystrophy [DMD/SMD] (Havens and Hastings, 2016).

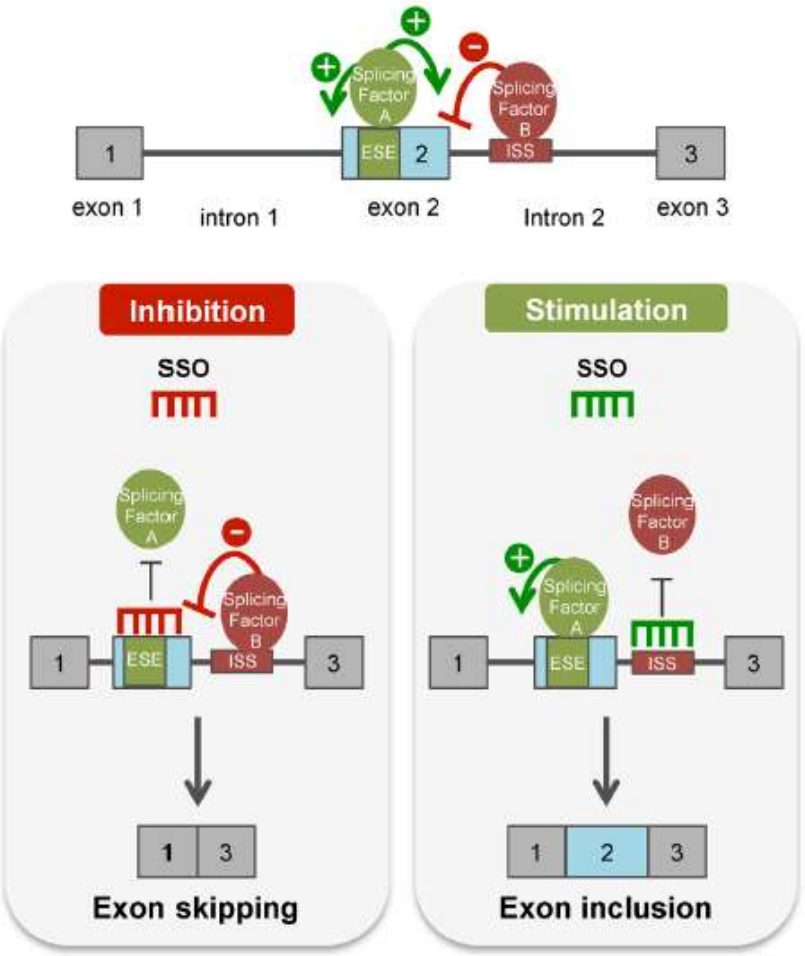

Figure 1. Spice-switching oligonucleotides [SSO] modulate splicing. Figure from reference (Havens and Hasting, 2016)

5.4 Challenges of siRNA and SSO nucleic acid therapy

siRNA and SSO have many things in common. In particular, both are involved in gene expression regulation. But also they carry important differences. These different drugs generate various strengths and disadvantages in drug development (Watts and Corey, 2012).

Even though unmodified duplex siRNAs were quite stable, chemical modification such as sisiRNA (siRNA made out of 3 strands) or shRNA (single-stranded hairpin type duplex) improved their properties tremendously (Sharma, Rungta and Prasad, 2014). Speaking of barriers in the delivery of RNA-modulating therapeutics, it is necessary to understand challenges at organ, tissue and cell level and to invest more effort in the evaluation of these. Even if distribution to diseased tissue was successful, it does not necessarily mean that siRNA/SSOs are internalized by the intended cell type (hepatocytes vs Kupffer cells in live, for instance) (Godfrey *et al.*, 2017). In serum, natural siRNAs could be degraded easily. Firstly, they have to face extracellular and after that intracellular nucleases. Also, siRNA has a significantly higher molecular weight when compared to conventional drugs based on small molecules. Unmodified siRNA has a half-life of approximately 15 min in the blood (Hickerson *et al.*, 2008). In contrast to viral vectors, until now only synthetic carriers ensured good protections against those nucleases. Interaction with serum proteins like albumin is not common, so this results in the rapid elimination of the drug through the kidney. (Juliano *et al.*, 2008). On the other hand, along with the liver, kidneys can accumulate a high amount of AON (antisense oligonucleotides) if distributed by systemic administration. AON dependent toxicities due to their chemical modifications, the immune response or entrapping in different tissues should be taken into account when evaluating the toxicology profile of drugs. It has been observed that the negative data and toxicology challenges, in general, will often not be available to the scientific community. There are many subcategories where all toxicities could be listed: pro-inflammatory mechanisms or effects of aptameric binding and many others. siRNA itself is involved

in the immune response by inducing interferon expression. Several pathways such a PKR [protein kinase R] and toll-like receptor (TLR) 3, TLR 8 and TLR 7 [found on dendritic cells and monocytes] could be entangled in stimulated production of proinflammatory cytokines. Although the exact process is not known, some modifications [e.g. 2'-*O*-methylation] resulted in reduced immune activity (Ozcan *et al.*, 2015).

Use of chemical modification, in this case phosphorothioate [PS] instead of the phosphodiester bond, led to increased half-life and the modified nucleic acid was rapidly distributed to peripheral tissue [this is one of many modifications possible, such as boranophosphate siRNA, 2'-F-RNA, LNA (locked nucleic acid), 2'-F-ANA, 2'-OMe/2'-OMEO and others]. Also, the delivery of those compounds has been improved. However, potencies were not as before. Consequently, these results forced the use of high concentrations siRNA or SSO, which led us to effect known as "off-target", one of the intracellular barriers known to us.

Conceptionally, siRNA/SSOs are designed to be highly target-specific. Reality is more complex. Due to the ability to tolerate some mismatches and to bind similar targets, AONs can lead to shutting down unpredictable numbers of genes. Furthermore, in mRNA recognition machinery key role play so-called 'seed regions'. They can be recognized with perfect complementarity, containing only 2-8 nucleotides, which makes unintended degradation even more efficient (Ozcan *et al.*, 2015).

Upon cellular penetration, which could be relatively poor because of the anionic nature of gene cargo, the next fundamental step which still needs to be overcome, is the endosomal barrier. To improve nucleic acid delivery, scientists have developed plenty of modifications that could be protonated in the endosomal environment with low pH and secure escape of AONs. The process is known as the 'proton sponge effect'(Godfrey *et al.*, 2017).

Despite the great potential of the antisense approach, still, considerable efforts need to be undertaken toward developing an efficacious delivery system. To date, one of the greatest successes has been archived using nanoparticle systems (McClorey and Wood, 2015).

5.5 Delivery strategies for siRNA and SSO

5.5.1 Gold nanoparticles for NA delivery

Compared to small-molecule drugs, nucleic acid therapeutics demand vehicles for adequate delivery as well as the protection from extra- and intracellular environment providing safe cellular uptake. To overcome these limitations, nanosized carriers for the delivery such as gold nanoparticles (AuNPs) came into the central focus of many biomedical fields including gene therapy in the first place. Gold nanocarriers possess numerous advantages as a reproducible synthesis with the possibility of changing gold surface properties and size range. There are many functional chemical groups with the availability of modification, which can be characterized precisely using selective assays. Furthermore, they can stay in narrow size distribution and probably most important would be their biocompatibility with different types of cells. It has been investigated not only the complexation of gold with gene material but also with a variety of antibodies, peptides and membrane ligands which could affect specific cell uptake or endosomal release (Shukla *et al.*, 2005; Lee *et al.*, 2008).

Even though gold has been used for centuries, it's colloidal nature is being intensively researched in the last 150 years. Gold nanoparticles present most stable metal nanoparticles with unique properties such as highly shape- and size-dependent electronic and magnetic features followed by optical properties (known as quantum size effect). These characteristics vary from bulk gold (Edwards and Thomas, 2007). Additionally, stabilization of AuNPs can be achieved with the anchoring of many known stabilizers (e.g. surfactants, citrate, peptides, dendrimer, etc.) or ligands such as oligonucleotides or antibodies. First, they should prevent aggregation in solution as well as in the bloodstream. Second, the functionality of NP can be altered intentionally. Frequently applied and the best stabilizers till now are thiolates, especially in case of conjugation with oligonucleotides. The use of these additional moieties can drastically

alter outstanding properties. Therefore, understanding of AuNP-chemistry can be essential (Giljohann *et al.*, 2010).

In the last few decades, a huge number of AuNPs syntheses were published. The most conventional method was introduced in 1951 by Turkevitch (Turkevich, Stevenson and Hillier, 1951) based on citrate reduction of HAuCl4 in water [Au(III) to Au(0)]. The citrate will be displaced through the establishment of a strong Au-thiol bond. The surface is now strong negatively charged and makes conjugation with positively charged PEI [polyethyleneimine]. The recent improvements in this method granted better size control in the range of 9-120 nm including better size distribution (Daniel and Astruc, 2004; Boisselier and Astruc, 2009; Giljohann *et al.*, 2010).

One of the most unique spectroscopic properties of gold is called surface plasmon resonance (SPR). The loss of light after passing through some medium can be caused by absorption and scattering. Light absorption is basically a transformation of photon energy into internal energy. Light scattering is a process that occurs when electromagnetic energy generates electron oscillations either at the same or at a shifted frequency. SPR can be understood as a collective oscillation of the free electrons on AuNp's surface. It is known that this oscillation is in correlation only with particular wavelengths/frequencies of the electromagnetic field [light] resulting in absorption in the visible range. This spectroscopic behavior was 1908 predicted by Mie's theory, wherein Gustav Mie solved Maxwell's equation of interaction between small nanoparticles and electromagnetic light (Amendola *et al.*, 2017). The SPR phenomenon, as well as SPR peak and bandwidth, depend strongly on NP shape, size [nanorods, nanostars, nanotriangles, nanocubes, nanorices, etc.], inter-particle distance, and surface. It is known that the width of SPR increases with the size reduction of NPs smaller than 25nm and vice versa if they are bigger than 25nm. Λ-max or SPR maximum is located between 517 and 570nm in NPs with a size of 9-99nm. Additionally, it can be influenced by temperature and dielectric constant of the medium surrounding it. Information provided by SPR is especially valuable in the determination of NP's characteristics in photochemistry and photophysics. In practice,

particularly it is used when it comes to the synthesis of gold conjugates. For instance, a layer of thiolate ligand can induce SPR to shift toward higher wavelengths through interaction with oscillated electrons. This occurs when NP size is changed but also if space between NPs is reduced according to electrodynamics modeling (Daniel and Astruc, 2004; Boisselier and Astruc, 2009; Giljohann *et al.*, 2010; Huang and El-Sayed, 2010).

Beside this feature, gold NPs include a variety of other advantages as relative simple labeling and imaging. For example, TEM [transmission electron microscopy] utilizes the high atomic weight of Au for the imaging of nanoparticles. An optical microscope detects AuNPs based on scattered light. There are also many other techniques like photothermal coherence tomography, fluorescence microscopy, X-ray computer tomography, etc.

To date, different shapes and sizes of gold NPs have been tested and it appears that no significant immunogenicity and cytotoxicity was observed (Lewinski, Colvin and Drezek, 2008; Boisselier and Astruc, 2009; Giljohann *et al.*, 2010).

5.5.2 Thiol reaction on the gold surface

To exploit all the advantages of gold NP, firstly it is essential to find a way to prevent natural aggregation of colloidal nanoparticles in saline solution and in the presence of biological molecules. Thus, anchoring gold's bioconjugates such as thiol molecules on the Au surface eliminates gold's tendency to aggregate. In previous studies (Joseph and Geckeler, 2009; Liu, Wang and Jiang, 2011) scientists created self-assembled monolayers with conjugates such as cyclodextrin and surfactants for the purpose of better dispersibility and stability. However, thiolate chemisorption resulted in strong thiolate bonds (40-50 kcal mol^{-1}, even stronger than Au-Au bonds) and they are considered as the best stabilizers in the gold passivation process. Compared to other thiol compounds [cystamine, dihydrolipoic acid, mercaptopropionic acid, glutathione, etc.], particularly thiolated PEGs shown great protection against the vascular immune system (Boisselier and Astruc, 2009).

Synthesis of thiol SAMs is a quite routine method and widely used. Simple exposure of thiol to clean a gold surface leads to clean, flat, and oxygen-free layers with the possibility of size control both in gas and liquid phase. Additionally, this method guarantees a monodisperse NP. In brief, after deprotonation of sulfhydryl [SH], thiyl radicals [$RS^{\cdot}$] will be formed. Finally, it all results in a covalent interaction between gold and sulfur. On another side, protonated SH-groups establish only coordination-type bonds [much weaker than covalent bonds] using sulfur electron pairs (Häkkinen, 2012).

But how strong are actually thiol bonds? In previous studies (Grandbois *et al.*, 1999; Skulason and Frisbie, 2000; Krüger *et al.*, 2002; Frei *et al.*, 2012) many investigations have been carried out aiming to quantify the strength of single covalent cond. The results demonstrated the rupture force of 1,0 to 1,5 nN. However, these values come from different experimental conditions and cannot be compared subsequently. Altogether, the formation of Au-S covalent bonds strongly depends exactly on these conditions such as pH, surface preparation methods/properties and interaction time.

The covalent bond rate was found to increase with increasing pH value on oxidized gold. Also, minimal reaction time for the formation of optimal Au-S bonds is around 3,0 seconds (Xue *et al.*, 2014; Vanegas, Scaiano and Lanterna, 2017).

5.6 Polyplexes for siRNA and SSO

5.6.1 Polyethyleneimine based polyplexes

Most cationic polymers are able to condense genetic material into smaller particles, inducing endocytosis through the negatively charged cell membrane. However, not all of them possess the same toxicity- and transfection profile.

One of the best known cationic, water-soluble polymers for gene delivery is PEI [polyethylenimine]. If fully protonated in aqueous solution, the density of positive charge, which is 20-25 microequivalents per gram, is incomparable with other polymers: every third atom in molecule is nitrogen, and one-sixth of them are positively charged at pH 7 (Neu, Fischer and Kissel, 2005; Gao, Kim and Liu, 2007). There are two configurations of PEI commonly used: BPEI [brached PEI] with approximately amine group ratio of 1:1:1 [primary:secondary:tertiary] and LPEI [linear PEI] with secondary amines excluding terminal ones (Von Harpe *et al.*, 2000). These positively charged atoms will interact with negatively charged phosphate in siRNA/SSO forming self-assembling particles through electrostatic interaction, known as polyplexes, which are based on non-covalent bonds. A huge number of PEIs are commercially available but not all are suitable for efficient transfection without toxicity effects on the organism. It has been found that the most suitable PEIs for gene delivery are in the range between 5 and 25kDa. Larger molecular weights exhibit more toxicity perhaps due to aggregation and smaller PEI has shown low transfection rate (Neu, Fischer and Kissel, 2005; Gao, Kim and Liu, 2007). The adequate complexation and transfection afterward depend not only on molecular weight but also on other characteristics such as the ratio of polymer to siRNA/SSO, the density of charge or buffer capacity, solvent properties and cell type (von Gersdorff *et al.*, 2006; Gao, Kim and Liu, 2007).

This polyethyleneimine mediated delivery platform grants oligonucleotide protection from degradation, cell uptake and endosomal release, especially in tumor tissue. It is likely that PEI's protonable amino groups are capable of protonating at a low pH

environment, causing osmotic swelling and rupture of endosomes realizing the transfer of genetic material into the cytosol (Günther *et al.*, 2011; Helmschrodt *et al.*, 2017). An approach like this demonstrated promising results in numerous studies worldwide (Akhtar and Benter, 2007; Höbel and Aigner, 2010; Wang *et al.*, 2015; Peng *et al.*, 2016).

5.7 Nanoparticle tracking analysis

NTA (nanoparticle tracking analysis) is a relatively new method for visualization and size quantification in a variety of nanoparticles suspended in liquids. The theoretic principle originates from 1991 (Qian, Sheetz and Elson, 1991) but implementation required advanced technology in many fields. NTA generates accurate and reproducible measurements for all kinds of nanoparticles in a wide range from 10 to 1000 nm. It is a practically automated method and does not request a lot of sample preparation time, except a diluting sample to optimal concentration. Additionally, all measurement settings can be manually adjusted (Wikipedia contributors, no date; Saveyn *et al.*, 2010).

Figure 2. The NS500, Malvern Analytic. Figure from reference (*NanoSight NS500*, no date)

Due to collision with liquid molecules, NPs are constantly in random motion so-called Brownian motion, which, together with the feature of NP's ability to scatters the light, represents a physical principle for size analyze. A specially designed illumination device [laser] is passing through the sample chamber, scattering the light of particles on its way. This scattered light comes first to microscope lenses giving the ability to visualize NPs in real-time. After that, pictures will be captured as a video via a CCD camera monitoring rapid particles individually. Usually, conventional CCD cameras shoot 60 frames per second making frame-by-frame tracking possible. Video clips will be stored and processed. In liquid, particle motion depends on size [r: (m)], the viscosity [η: (Pa.s)] of the dispersant and temperature [T: (K)]. Tracking particle's change of position in two-dimensional space allows evaluating the speed of motion or diffusion constant [Dt: (m^2/s)]. Since temperature is constant inside of NTA device and solvent viscosity is known as well as diffusion constant, it is simple for software to evaluate particle hydrodynamic diameter using Stokes-Einstein equation (NanoSight Ltd., Minton Park, Amesbury, Wiltshire SP4 7RT, 2012; Schützhofer, 2018):

$$Dt = \frac{KB \times T}{6\pi \times \eta \times rh}$$

[KB= Boltzmann's constant (m^2kg/Ks^2); rh= hydrodynamic radius (m)]

5.8 Dynamic Light Scattering

DLS or Dynamic Light Scattering (also known as photon correlation spectroscopy) is one of the most popular light scattering techniques for measuring the particle size in the nanometer range (AG, 2019). The basic principle remains the same as in NTA: the constant collision between particles and solvent results in a random movement of particles in all directions. These interactions produce a certain amount of energy, which will be transferred to the next particle and affects them differently depending on size. Consequently, small particles will be diffusing faster than larger. As mentioned previously, such motions depend on the size, temperature, and viscosity of the solvent. Since the accurate temperature and viscosity are known, it's simple to calculate the hydrodynamic diameter by measuring particle speed (see NTA paragraph). The correlation is described by the Stokes-Einstein equation (GmbH, no date; Wikimedia Foundation, no date).

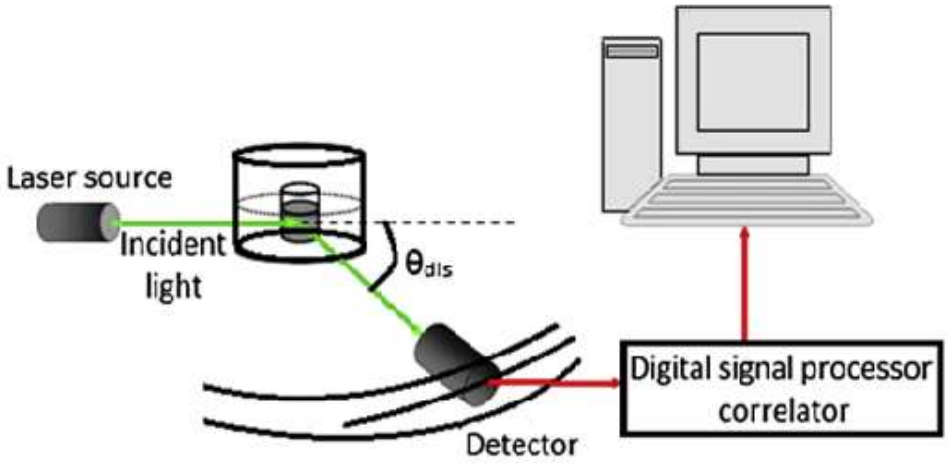

Figure 3. Schematic illustration of DLS. Figure from reference (Sakho *et al.*, 2017)

When a laser beam encounters macromolecule in a cuvette, the light will be scattered in all directions. This scattered light intensity is being monitored over time by fast

photon counter [detector] changing constantly with respect to particle size and time; smaller particles are moving at a higher speed which implies faster fluctuation [faster decay] and larger particles slowly and vice versa. It is important to note, that surface structure, as well as the ionic concentration of the solvent, can significantly change apparent particle size. Analysis of time-dependent fluctuations of scattered light generates diffusion rate [Dt], which relates directly to the average particle size [Stokes-Einstein equation] (Ltd, no date; Wikimedia Foundation, no date; Sakho *et al.*, 2017).

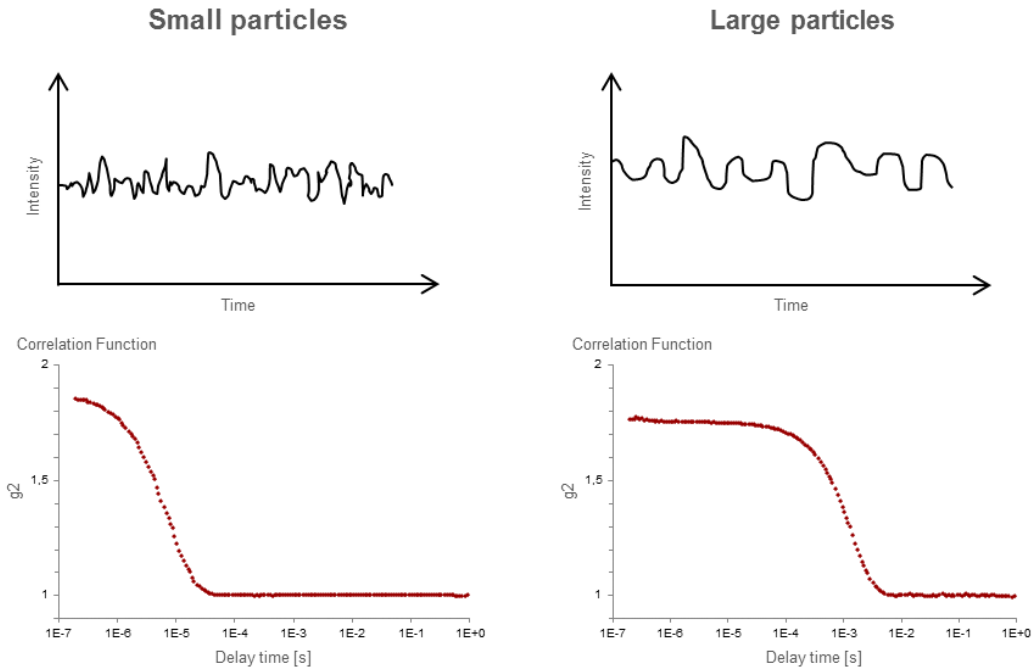

Figure 4. Fluctuation comparison of scattered light with respect to the time/decay of small and large particles. Figure from reference (GmbH)

Additionally, the Zetasizer Nano ZS is capable of measuring zeta potential, which is a key indicator for stability assessments in colloidal suspensions (Uskoković *et al.*, 2011). Upon applying a voltage in a cell with the sample, AuNPs move to the electrode with the opposite charge. The particle velocity will be estimated as a function of voltage (Doppler technique), moving particles scatter light at a frequency proportional to their speed. This velocity, measured at multiple voltages, will be used to determine the zeta potential (nanoComposix, 2019). In comparison to NTA, DLS does neither visualize nor calculate the approximate particle concentration. On the other side, DLS is a time-saving technique, does not demand skilled operators or additionally adjustments for analyses. More details relating to a comparison between DLS and NTA can be found in reference X (Filipe, Hawe and Jiskoot, 2010).

5.9 Characterization of gold NPs by UV-Vis spectrometry

As mentioned previously, gold nanoparticles are one of the essential compounds in nanotechnology mostly due to their SPR feature, among all other things like biocompatibility, simple surface modifications, etc. However, the application of gold NP is strongly dependent on concentration, size, and aggregations defining their biological properties (Amendola and Meneghetti, 2009).

The commonly used method for determining structural morphology and accurate physical size of AuNP is Transmission Electron Microscopy (TEM). Nevertheless, the monitoring of nanoparticles size in real time, concentration and aggregation states will not be provided by TEM (Murray, Kagan and Bawendi, 2000). Additionally, sample preparations are demanding and time-consuming. On the other side, UV-VIS (ultraviolet-visible) spectroscopy is one of the most simplified techniques to study the optical properties of the materials. UV-Vis data will be recorded in the range of 300 to 800 nm. It is routinely employed in most laboratories, measuring itself is very fast and will not cause any interactions with the sample.

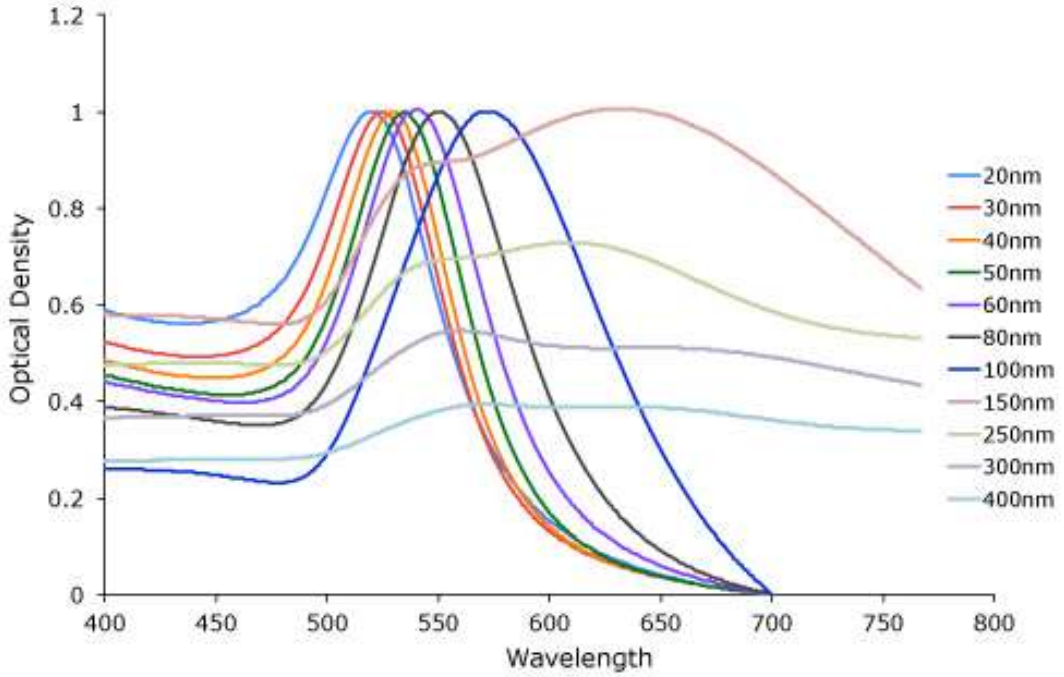

Figure 5. SPR red-shift of size-dependent gold nanoparticles. Figure from reference (Inc., 2019)

Importantly, all parameters like concentration, size, and aggregations are measurable using UV-Vis spectroscopy in a short time. So far, for estimating theoretical values of particle size many calculation models and programs are presented (Khlebtsov, 2008, 2008; Amendola and Meneghetti, 2009; C. Martínez *et al.*, 2013; Haiss *et al.*, 2015). They are all based on Mie theory and Beer's Law, where it was assumed that all AuNP's are monodispersed. Previous studies strongly indicated that the SPR position depends on various factors like particle shell and their chemical or physical interactions, dielectric properties of the solution, the distance between particles, etc. (Amendola and Meneghetti, 2009). And altogether, they can affect results obtaining the inaccurate average diameter of gold nanoparticles at the end. So this technique should be considered just as an alternative tool. Using the TEM or DLS instrument, the best accuracy can be achieved (Rahman, 2016). In this thesis, UV-Vis data supplies primarily with pre-coating and after-coating information, revealing if coating actually

happened or not. Moreover, aggregations will be noticeable in the spectrum if occurred.

5.10 Copper-assay

Cu-assay offers a quantitative analysis of PEI, ether in the presence of an associated oligonucleotide/gold or PEI alone, using the spectrophotometric method. Because LPEI does not carry any chromophores, detection would not be possible by ordinary spectroscopy. In order to enable it, copper (II) ions will be added in the PEI solution, forming a dark blue cuprammonium complex. For the best reproducibility, the ration 1:5 N/Cu in aqueous solution was chosen (Ungaro *et al.*, 2003). This complex displayed two absorption bands with maxima at 285 nm and 630 nm (Wen *et al.*, 2017). Later on, results exhibit a better linear relationship (r^2=0.9997) between PEI amount and absorbance working at 285 nm, which will be applied for further experiments. Furthermore, optimal concentration was found in a range of 5.0 to 50.0 mg ml^{-1}. Overall, this method ensures many advantages like high sensitivity and selectivity, fast and simple detection, and etc.

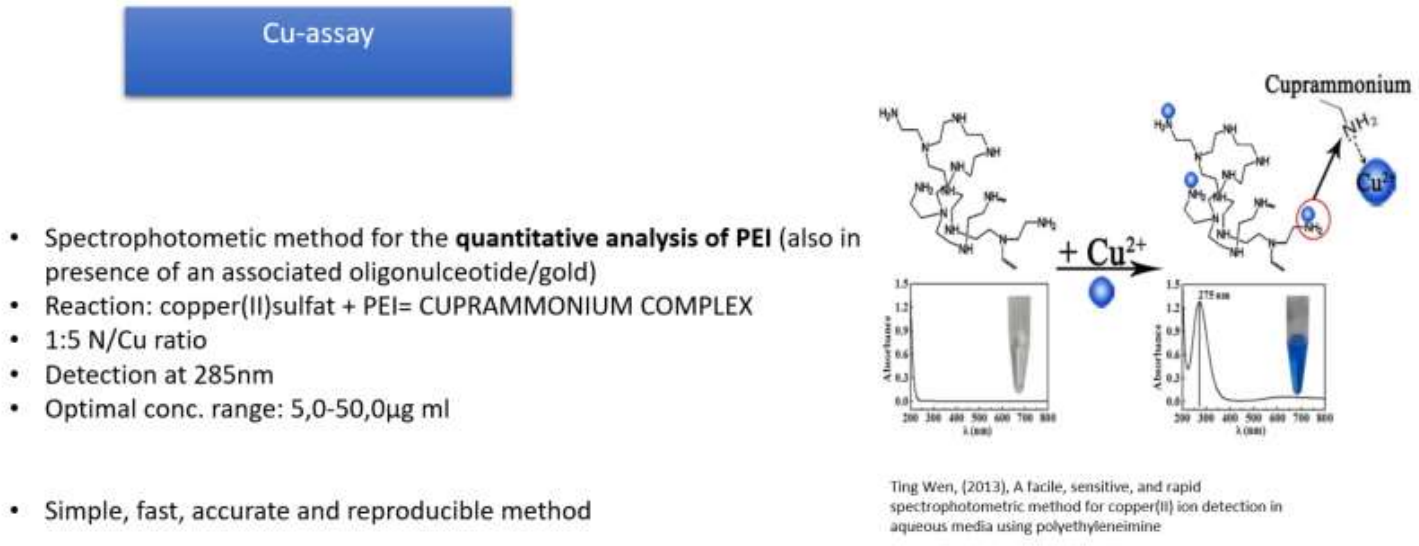

Figure 6.A basic explanation of Cu-assay. On the right side presented is a reaction with BPEI

5.11 Gel retardation

Gel retardation assay, also known as electrophoretic mobility assay [EMSA] is a commonly used electrophoretic method to study different interactions between nucleic acids and any materials that bound with it, such as proteins, polymers, various nanoparticles, etc. (Park and Raines, 2008; Wikimedia Foundation, 2019). In practice, most investigated are DNA-protein or RNA-protein interaction. However, this method of electrophoretic separation is based on agarose- or polyacrylamide gel where molecules migrate through pores of the gel at diverse speeds. The speed at which molecules (or complexes) 'shifting' in gel depends strongly on their size and charge, eventually also on particle/molecule shape or gel charge (Wikimedia Foundation, 2019). Consequently, unbound fragments or free nucleic acids are moving faster comparing with corresponding complexes of larger structures. This approach is also capable of quantitatively and qualitatively estimating the complexation rate by comparing different ratios of compounds. Besides that, a wide range of oligonucleotides starting from short oligonucleotides to thousands of nucleotides or bp [base pairs] as well as single-stranded/duplex/triplex nucleic acid structures or circular DNA can be uncomplicatedly detected by EMSA. Along the side of all these advantages, disadvantages like the possibility of dissociation during electrophoresis or even increase of stability of complexes in gel should be considered (Hellman and Fried, 2007). Finally, valuable aid for the detection of nucleic acids is ethidium bromide [EtBr], powerful mutagen and teratogen, which is still widely used even though many other safer DNA dyes are commercial now. The DNA can be simply visualized by intercalating EtBr into DNA/RNA molecules and illuminated with a UV light source [for instance: ChemiDoc™ MP]. It is likely that this binding results in a change of weight, charge, and structure of molecules, that must be taken into account (Sigmon and Larcom, 1996; KGaA, 1999).

Figure 7. ChemiDoc™ MP.

6. Aim of the thesis

The main aim of the thesis was the synthesis and detailed biophysical characterization of cationic gold nanoparticles. This was achieved by coating citrate stabilized gold nanoparticles with thiolated-LPEI by thiol based adsorption on the gold NP surface. The synthesis of nanoparticle functionalized polyplexes with a different combination of formulations is in the interest of establishing reproducibility in the coating process. Towards this, first the gold nanoparticles were characterized by dynamic light scattering, nanoparticle tracking analysis and UV-Vis spectrophotometry. Then these gold NPs were used for coating with LPEI-SH and the aim was to quantify the amount of LPEI-SH on gold by direct and indirect methods of quantification. UV-Vis spectrophotometry was done to establish a correlation between SPR shifts and LPEI loads bound on gold. Finally, the goal was to use these optimized cationic gold nanoparticles for complexation of SSO to generate SSO based auropolyplexes. An additional aim of the thesis was to calculate and test optimal polyplexing conditions of PEI [LPEI and BPEI] with siRNA with respect to the number of nitrogen and phosphate atoms considering the time as the factor that can influence the process.

7. Materials and Methods

7.1 Chemicals and plasmids

7.1.1 Reagents, chemicals, and buffers

- Ultra-pure water (= MQ-H2O; provided by Arium Pro VF ® (Sartorius))
- Ethidium bromide (provided by Prof. Winkler workgroup, University of Vienna)
- LPEI-SH 5kDa (from batch 170918; prepared by Simon Decker)
- HEPES (4-(2-hydroxyethyl)-1-piperazineethanesulfonic acid) (AppliChem)
- 20x Sodium borate (SB) buffer (4.8% boric acid, 0.8% NaOH, adjusted to pH = 8.0-8.2)
- 1x SB buffer (Dilution of 20x stock solution in MQ-H2O)
- HBG buffer (20mM HEPES, 5% Glucose, pH = 7.4, sterile filtrated)
- FastRuler Middle Range DNA Ladder™ (Thermo Scientific)
- MassRuler DNA Loading Dye™ (6X) (Thermo Scientific)
- Agarose DNA Pure Grade (VWR)
- Copper(II) sulfate (Merck)
- 25kDa BPEI (Sigma Aldrich CAS Number 9002-98-6)
- Ethanol (AppliChem)

7.1.2 Nucleic acids

- siRNA (The oligonucleotides used in this work were supplied by GSK (Glynn Williams, Jonathan Northall) as part of their contribution to the EU/EFPIA Innovative Medicines Initiative Joint Undertaking COMPACT)

- AF750-SSO (The oligonucleotides used in this work were
- supplied by GSK (Glynn Williams, Jonathan Northall) as part of
- their contribution to the EU/EFPIA Innovative Medicines Initiative Joint Undertaking COMPACT

7.2 Devices

- Microwave
- Electrophoresis power supplies (PowerPac™)
- Microcentrifuge, refrigerated, Micro Star 17R (VWR Collection)
- Nanosight NS 500 (NanoSight Ltd.)
- Magnetic stirrer (Heidolph Instruments)
- Arium Pro VF ® (Sartorius)
- ChemiDoc MP™ XRS+ Molecular Imager (Bio-Rad)
- NanoVue Plus Spectrophotometer (Biochrom)
- GeneQuant 1300 Spectrophotometer (Biochrom)

7.3 Materials

- Eppendorf Micropipettes (2 - 20µl, 20 - 200µl, 100 - 1000µl) (Eppendorf Research Plus)
- Centrifuge Tube 15 ml (CT-15) (Starlab)
- Centrifuge Tube 50 ml (CT-50) (Starlab)
- Eppendorf tubes/reaction tubes (various sizes) (Nerbe Plus)
- Pipette tips (various sizes) (Nerbe Plus)
- Syringe filters, cellulose acetate, 0.22 µm (VWR)
- UV-cuvette [semi]-micro (Brand GmBH)

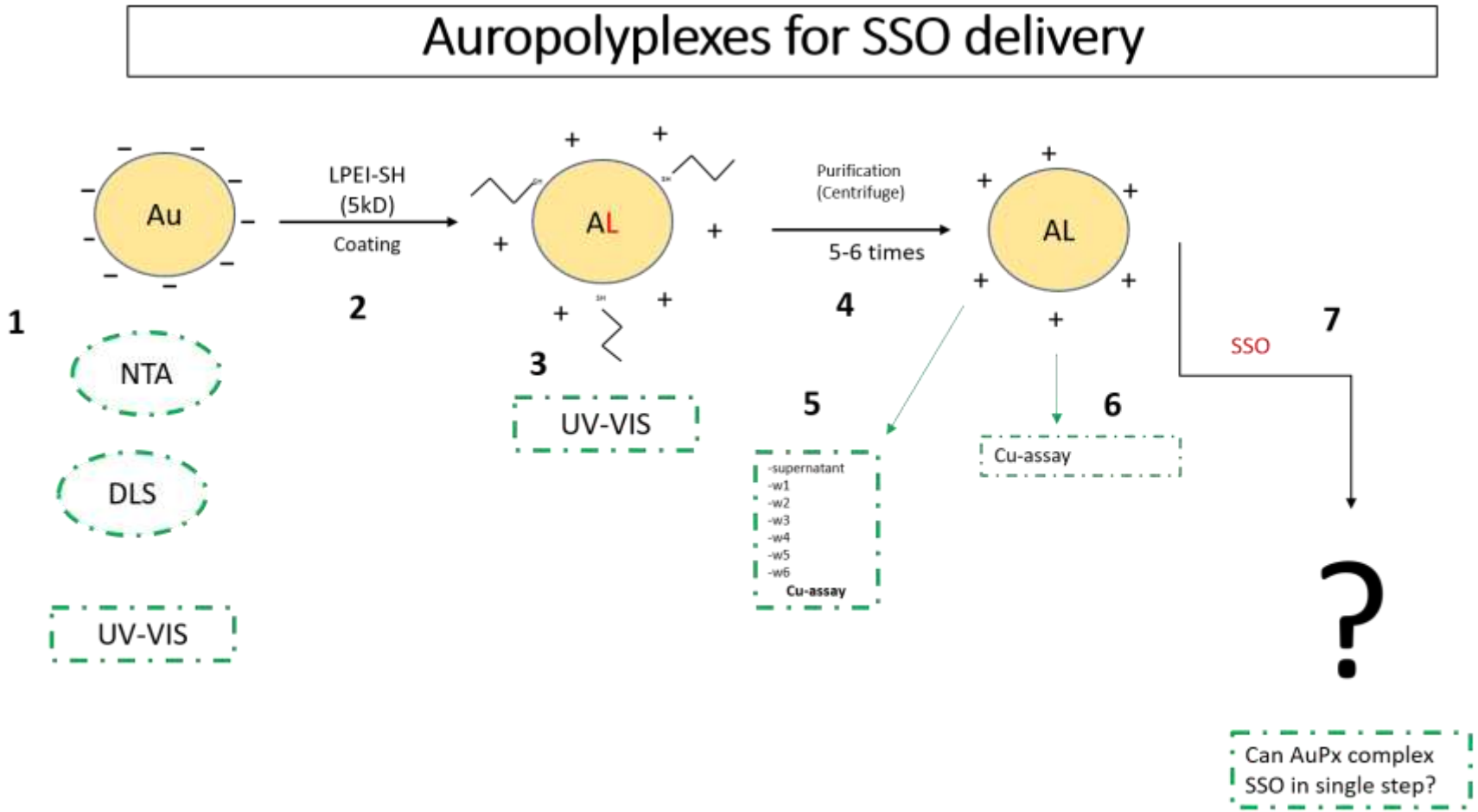

7.4 Workflow overview

Figure 8. Overview of SSO auropolyplexes synthesis. Number represents order in which steps are accomplished

7.5 Characterization of gold NPs by dynamic light scattering and nanoparticle analysis

To determine if aggregation occurred in a colloidal gold solution, the naked-eye observations were made first. If the solution is unstable, particles stick to each other forming spontaneously sediment at the bottom. Gold particles cannot be disrupted easily (or even irreversibly aggregate) but once they settled, it comes to color change in the liquid from pink to dark purple/blue. This change is clearly visible. And in our case, there was no aggregation observed in any of 9 batches of gold which makes them potential candidates for further coating.

Figure 9. Homogenous gold solution vs aggregated gold nanoparticles. Figure from reference (Inc.,). The difference is observed with the unaided eye.

Further, gold nanoparticles sizes from all batches were evaluated using NTA, using NanoSight NS500 [software 3.2 NanoSight]. The optimal NP number range per

measurement was from 5 to 100 NPs (Ltd., 2013). Therefore, each sample was diluted 1:100 (10 µl of AuNp batch + 990 µl of MiliQ).

As the diluted sample is loaded into the sample chamber, NPs scatter the laser light. This scattering pattern is captured by a CCD camera and stored as raw data. In order to obtain a particle's velocity, this data will be analyzed frame by frame for each particle using NanoSight NTA 3.2 analytic software. Finally, using Einstein-Stock equivalation [detailed information of NTA can be found in the introduction under section NTA], mean hydrodynamic diameter[MHD] can be calculated as well as other statistical parameters; standard deviation, mode, etc. All results presented in graphs can be found in the Results section [Figure 11 and 12].

7.6 Characterization of gold NPs by UV-Vis spectrometry

Additional characterization by spectrophotometry is necessary in order to monitor eventual changes in particle size or coating shells. First, SPR of all batches will be localized and kept as a reference value [Figure 10] for further investigations. In this case, it will be utilized primarily as an indicator of AuNPs coating with LPEI [linear polyethylenimine].

When working with gold, keeping the workspace clean and pre-rinse [3x] of pipette tips were obligatory in each step. From vigorously stirring Au solution 80 µl were taken each time and transferred in micro UV cuvettes with standard 10mm light path. The MiliQ water served as a reference. It was taken at least 2 [more needed if aberration was bigger than 1nm in maximum] spectra for each colloid suspension in the range from 400 to 700 nm. All spectrums were recorded with GeneQuant 1300 Spectrophotometer.

7.7 Coating of gold NPs by LPEI-SH and characterization by UV-Vis spectrometry

The coating procedure was done in a new 20 mL snap-cap vials with a small magnetic stir bar inside. Since colloidal gold is susceptible to corrosion, magnetic stir bars cleaned in aqua regia (HNO_3+3 HCl) and plastic stir bar retriever were used to avoid contact with metal. All glassware has to be pre-rinsed a few times with MiliQ too. To obtain colloidal stability, before starting with actual coating, pH was adjusted above 8 by adding 1 M NaOH in 2 µl portions at room temperature. Thus stirring it with a magnetic stirrer, pH has been checked using pH indicator. The coating was performed under vigorously stirring, LPEI-SH (5kDa; 13.635 mg/mL) [for each experiment, fresh LPEI stock] was added dropwise using 200 µl pipette [it has been experimented with adding all at once too]. The coating was completed within a minute and stirring was continued for another 24 hours. If coating happened, the color of suspension changed from pinkish to purple in the first minute or two and this assertion could be checked using UV-Vis spectroscopy. On the other side, if aggregation developed, sedimentation would take place immediately. However, to estimate to what extent coating succeeded, comparison with initial SPR bands was necessary.

7.8 Purification of AL

The coated gold nanoparticles [AL] are purified by centrifugation. The aim was to remove excess LPEI-SH and to quantify it. After coating, the nanoparticle suspension is transferred in 2 mL reaction tubes, each containing 1 mL of suspension. The temperature on [device] was adjusted to 4 °C. According to the book 'Nanotechnology for Nucleic Acid Delivery: Methods and Protocols' (Maria Dusinska, Zuzana

Magdolenova (auth.), Manfred Ogris, 2013), the optimal settings for particles with 50-60 nm diameter are the centrifugal force of 5,000 x g in 10 minutes duration. After each centrifugation, supernatant/washes [900 µl] were removed extra cautiously in CT-50 and stored at room temperature, the pellet was washed and vortexed with another 900 µl of MiliQ. Taken together, supernatant and six washes [wash 1,2,3,4,5,6] are collected for each experiment.

7.9 Quantification of LPEI-SH on AL

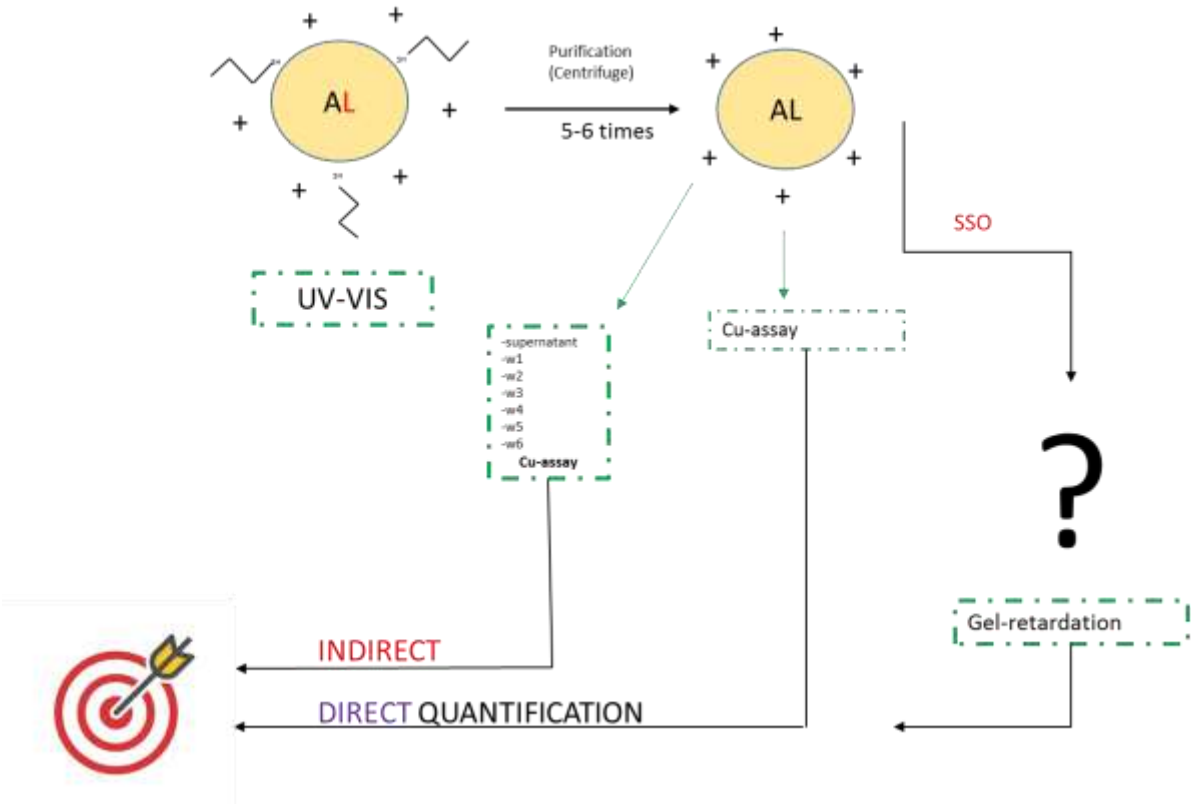

Figure 10. Schematic representation of LPEI quantification with respect to the whole process of auropolyplexes synthesis. Firstly indirect quantification was conducted [presented in red] followed with direct quantification using Al solution [presented in purple].

Following two experiments with Cu-assay, in both, supernatant/washes and AL solutions are a method of quantitatively determining the concentration of LPEI-SH in ultra-pure water. Quantification in supernatant and washes will be labeled as indirect quantification and in AL solution as direct quantification.

7.9.1 Indirect quantification

This assay is based on protocol made by Simon Decker which was established initially in the work of Ungaro (Ungaro *et al.*, 2003).

For all experiments, the same Cu^{2+} solution has been used [100 ml of Cu^{2+} solution contains 23 mg of $CuSO_4$ dissolved in 0.1 M Na-acetate buffer with pH 5,4]. To generate the standard curve, LPEI solutions are made in different concentrations starting from 10 µg/mL to 100 µg/mL with a final volume of 100 µL that will be diluted 1/125 [if needed, additional adjusting of pH with 1 M HCl]. This curve [Figure 12] ensures a linear correlation between absorption and LPEI concentration and it is crucial for calculations. In order to obtain good accuracy and reproducibility, standard solutions, as well as all samples, are analyzed in duplicates. On GeneQuant 1300 Spectrophotometer absorption wavelength was set on 285 nm and blanked against 40 µL of Cu^{2+} solution mixed with 40 µL of MiliQ. After mixing the sample/wash [40 µL] with Cu solution [40 µL], it has waited approximately 5 minutes till the absorbance of the Cu-LPEI chelate reached the maximum value and then measured.

Next, the average calculated from measurements was plotted on the standard curve graph using excel commands and LPEI concentration has been determined. For supernatant and wash 1 dilution steps were necessary [1/10 and 1/2].

7.9.2 Direct quantification

In direct quantification, the procedure stays very same as in indirect. Pre-rinsing of all glassware/tips that come in contact with AL solution is mandatory as well as vortexing it before taking an aliquot. However, the 'sample' here is the AL solution instead of supernatant/washes. Therefore, a purified and concentrated solution of AL was used in this assay. The aim is to quantify the amount of LPEI directs on gold NP using UV-VIS spectrophotometry absorption of the cuprammonium complex. In this case, multiple blanking is needed. Since multiple blanking, is not possible on the device itself, blanking was done in MS Excel. To get rid of Au absorption in 285 nm region, 40 µL of MiliQ with 40 µL of Au solution were mixed and measured and later subtracted from the main absorption [40 µL of AL solution + 40 µL of Cu reagent]. This represents the first blank, also labeled as NP blank. The second blank or reagent blank [40 µL of MiliQ + 40 µL of Cu reagent] will eliminate absorption from Cu reagent alone at 285nm. Finally, to evaluate the accurate amount of LPEI in µg, both blanks were subtracted from the main absorption [reaction time remains 5 minutes]:

$$LPEI\ on\ AL = [AL\ NPs + Cu\ reagent] - [NP\ blank + reagent\ blank]$$

This result was used for plotting in excel on standard cure, which is the same for indirect and direct quantification. It is important to notice that concentrated or low diluted AL solutions couldn't be used since absorption was too high. On the other side, a high dilution factor led to unreliable results [Figure 21]. The detectible window for a dilution rate of AL depends on the formulation and concentration rate after purification. Thus it varies from experiment to experiment.

7.10 Gel retardation of SSO by purified AL

7.10.1 Procedure: Gelation

Since all equipment for gel electrophoresis is contaminated with EtBr, extra caution is necessary when working with this chemical. It also needs to be ensured that the electrophoresis unit [gel box, gel plate, and well comb] are clean and dry before starting with the experiment. Afterward, all parts will be set together with respect to in the position of the anode and cathode, leveling it at the same time. The gel retardation process request that all components are free of nucleases which can degrade genetic material involved. In the first place, 1.8g of Agarose pure grade will be mixed with 120 mL 1xSB buffer [sodium borate buffer], making 1.5% agarose gel in the given volume. SB buffer maintains the pH at a constant value and provides plenty of ions, which are essential for electricity flow. This mix can be dissolved doing microwave for 3-4 minutes, thoroughly swirling every 30-45 seconds as solution heats up [overboiling can alter the percentage of agarose in gel!]. When the solution is fully liquid and clear, it has to cool down for another 30 sec. and then 4.2 µL Ethidium Bromide (10mg/mL) will be added quickly swirling Elenmayer flask gently. Now hot liquid can be poured carefully in casting tray with well-comb, avoiding bubbles. Then it comes to polymerization, which usually takes about one hour.

7.10.2 Procedure: Electrophoresis

After gelation of the agarose solution, the comb has been detached and the gel was moved in the electrophoresis chamber. This chamber will be now filled with a 1xSB buffer until the whole gel is covered. Afterward, samples were loaded carefully and the electrophoresis tank was connected to a power supply. And yet, two types of experiments can be distinguished:

1. Gel retardation of siRNA by LPEI/BPEI
2. Gel retardation of SSO by purified AL

In the case of gel retardation of siRNA by PEI, along with sample wells, reference bands with the pure siRNA and DNA ladder have been included. To keep samples on the bottom of wells and to ensure visual tracing of generic material, loading dye [4.2 µL] was added to the sample [20 µL] before loading it into wells. Now, the voltage was adjusted to 100V and electrophoresis was running for the next 45 minutes.

If the coating of AuNP happened, the complexation of AL with SSO was investigated. In the previous experiment, before this complexation, optimal SSO concentration in gel retardation was determined, which is 500 ng per well [results presented in the Results and discussion section]. In the gel retardation of SOS by AL, in contrast to siRNA/LPEI, no loading dye was used, but 60 % glycerol instead [4 µL]. And to ensure reference here, the SSO band [500 ng of SSO] and glycerol were involved as a control. After placing the lit on top, wires were connected into slots on the control unit and the device switched on. The gel was running at 80V for 12 [+20] minutes.

Immediately after starting the run, the current flow will produce bubbles at the electrode, which indicates that the device works properly.

7.10.3 Procedure: Imaging

And yet, after electrophoresis, the gel will be placed centrally on the transilluminator into ChemiDoc MP Imaging System. After login, the image size, as well as chemiluminescence under blots must be selected [EtBr]. The region of interest can be selected manually too [important for excluding extremely intense areas from

quantifying]. In the exposure menu, exposure time has been entered manually starting from 0.5 to 6.0 sec. for each capture. Additionally, auto-detection with optimal exposure was used for each gel, recruiting a full dynamic range of the instrument. All captured images will be saved automatically and can be exported. In final, for each gel, there is a minimum of 5-6 images for analyses.

7.11 Preparation of polyplexes

For the purpose of polyplexing, NC siRNA [conc. 20 µg/ml] was utilized. Both siRNA and LPEI/BPEI were stored at -80°C and dissolved in nuclease-free water. These polyplexes (PPx) were generated in HBS (HEPES buffered saline) buffer using a technique known as flush-pipetting. Before actually polyplexing, LPEI/BPEIs in different amounts were dissolved in HBS, depending on N/P ratios [first set of reaction tubes with a total amount of 10 µL]. In parallel, siRNA was mixed with HBS, always 4 µL of siRNA with 6 µL of HBS [second set of reaction tubes]. The entire calculations were performed using excel spreadsheets provides by Dr.Sami, which enabled automatic estimation of LPEI/BPEI amounts based on N/P rations [concentration of siRNA was constant as described above]. Homogenization was archived by finger punching of reaction tubes (1.5 mL) and by pipetting up and down a few times. The first set of reaction tubes was vortexed regularly and then all reaction tubes underwent spinning down. After the pipette was set to higher volume [approximately 15 µl] and LPEI-HBS was soaked up, the air was realized out of the tip. Carefully it was dipped in the siRNA-HBS solution and pipetted quickly 40-50 times up and down soon as it touched the liquid [flash-pipetting]. During the whole process, the formation of bubbles must be avoided. Normally, PPXs stay stable 30 minutes to one hour, before they tend to aggregate.

8. Results and Discussion

8.1 Overview of tested parameters

All of the following experiments fall within the scope of this thesis and were successfully carried out (the list of failed experiments can be found in Table 9 in Appendix):

Experiment	Batch	AuNP volume used (ul)	LPEI-SH volume added for coating (ul)	UV-Vis SPR shift	Total LPEI-SH amount added for coating (µg)
Exp. 1	1	10076.35 µl	923.65 µl	2 nm	12593 µg
Exp. 2	3	5038.18 µl	461.825	10 nm	6296.9 µg
Exp. 3	7	2500 µl	461 µl	2 nm	6296 µg
Exp. 4	8	2500 µl	923.65 µl	1 nm	12607.82 µg
Exp. 5	8	5000 µl	461 µl	1 nm	6296 µg
Exp. 6	8	5000 µl	923.65 µl	0 nm	12607.82 µg

Table 1. Overview of successful coating experiments. It includes all data relevant to the coating formulation: volume of gold solution and volume of LPEI, which was used for coating afterward and finally results of each experiment expressed in SPR shift.

Auropolyplexes as potential nano-transporter are already reported in our previous work. In this work, detailed biophysical characterizations were conducted with the ultimate goal to produce functionalized auropolyplexes and quantify the LPEI amount needed for it.

8.2 Biophysical characterization of gold NPs by nanoparticle analysis and dynamic light scattering

In figure 11 and 12 presented are average particle diameters (in nm) measured and calculated following instructions described in Material and methods section related to their concentration in ml for all batches used. All tested batches exhibited hydrodynamic diameter in the range of 54.5nm to 56nm (mode).

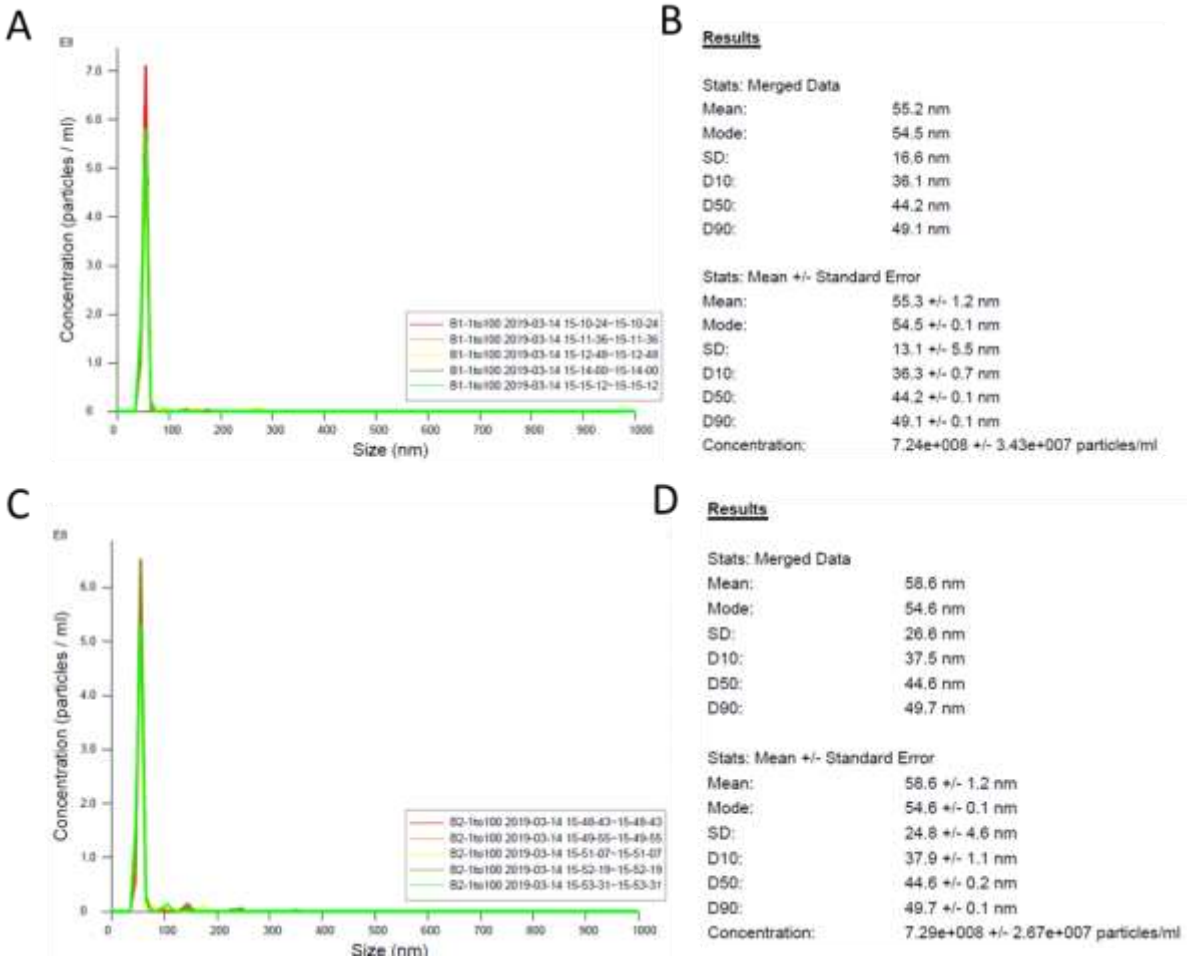

Figure 11. NTA based size distribution of different batches of gold nanoparticles. Size distribution profiles (A,C) and results (B, D) are shown for batch1 (A-B), batch2 (C-D).

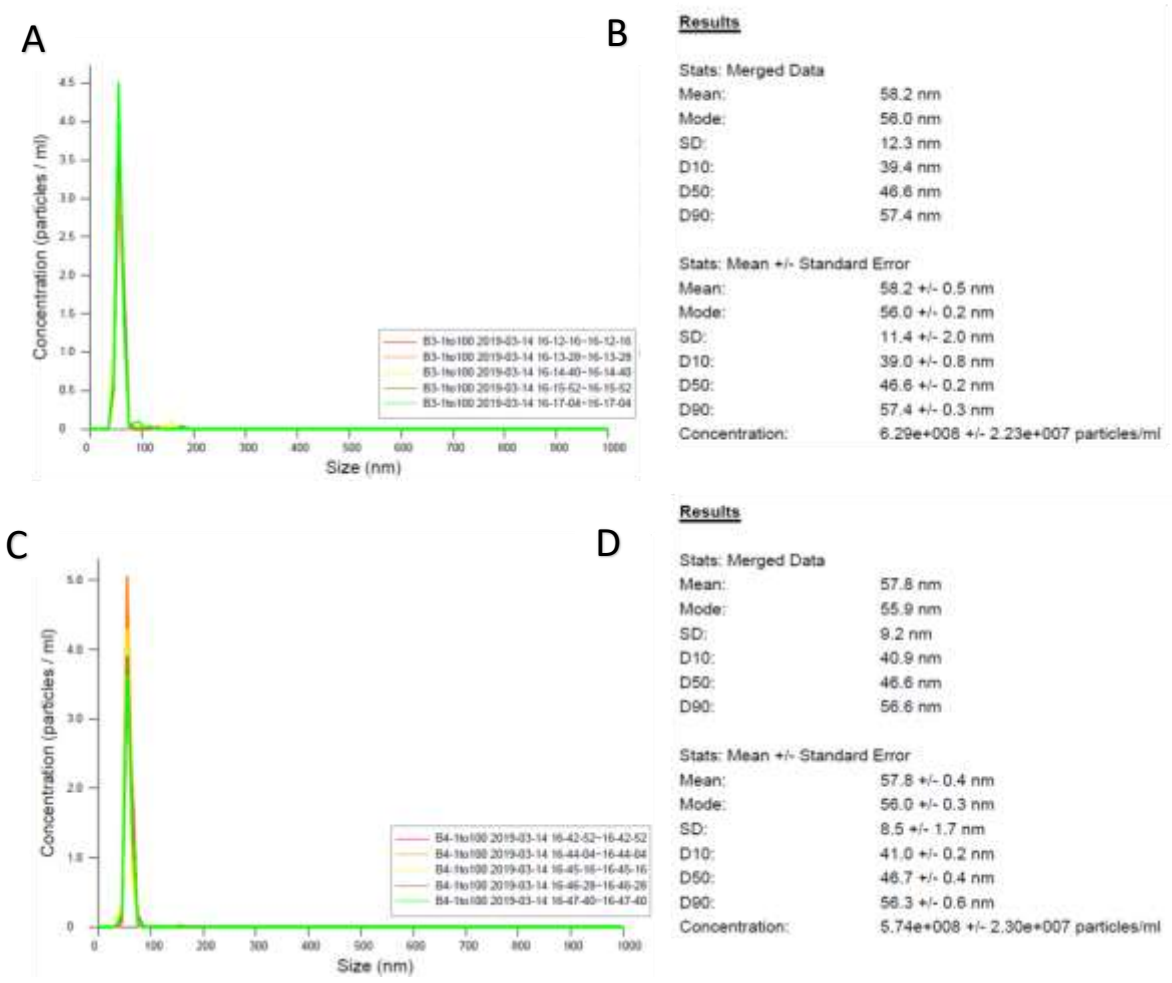

Figure 12. NTA based size distribution of different batches of gold nanoparticles. Size distribution profiles (A, C) and results (B, D) are shown for batch3 (A-B), batch4 (C-D).

As shown above, the MHD of the first 4 batches was around 57.45 nm and there was no aggregation observed. For comparative purposes, gold nanoparticles were characterized using DLS and results were compared with NTA data in Table 2. This time, the dilution rate was 1:10 instead of 1:100.

	DLS (average of all 3 measurements)	**PDI** Poly-dispersity-index (average)	**NTA** (average of all 5 measurements)
Batch 1	60.50 nm	0.341	55.2 nm
Batch 2	76.65 nm	0.322	58.6 nm
Batch 3	68.73 nm	0.454	58.2 nm
Batch 4	64.82 nm	0.442	57.8 nm

Table 2. DLA- vs NTA mean hydrodynamic diameter of the same gold NP solutions.

In conclusion, the mean hydrodynamic diameter of DLS measurements was 17% bigger than the same measurements done by NTA. However, this was expected with respect to the different measurement principles. The overall goal of this experiment was not to compare these two methods but to corroborate NP's size from two different techniques.

8.3 Characterization of gold NPs by UV-Vis spectrometry

These spectrums below were recorded with GeneQuant 1300 Spectrophotometer and the peak/SPR was clearly visible in the range from 531-542 nm for all tested batches [Figure 13 and 14]. For the purpose of comparison for each spectrum, the maximum was estimated separately [Table 10, in Appendix].

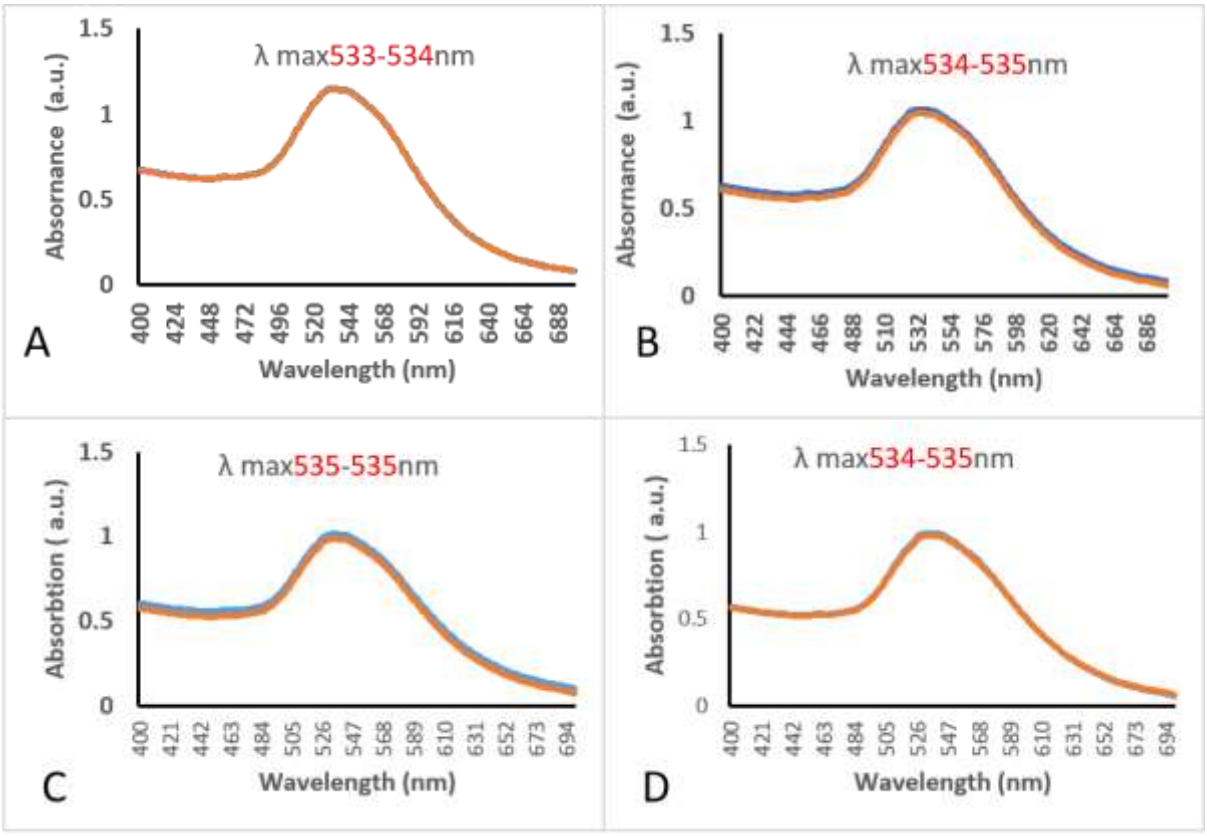

Figure 13. UV-Visible spectra for analyzed gold nanoparticles showing the position of surface plasmon resonance peak bands [λmax] for different batches (Batch1-A, batch2-B, batch3-C, batch7-D)

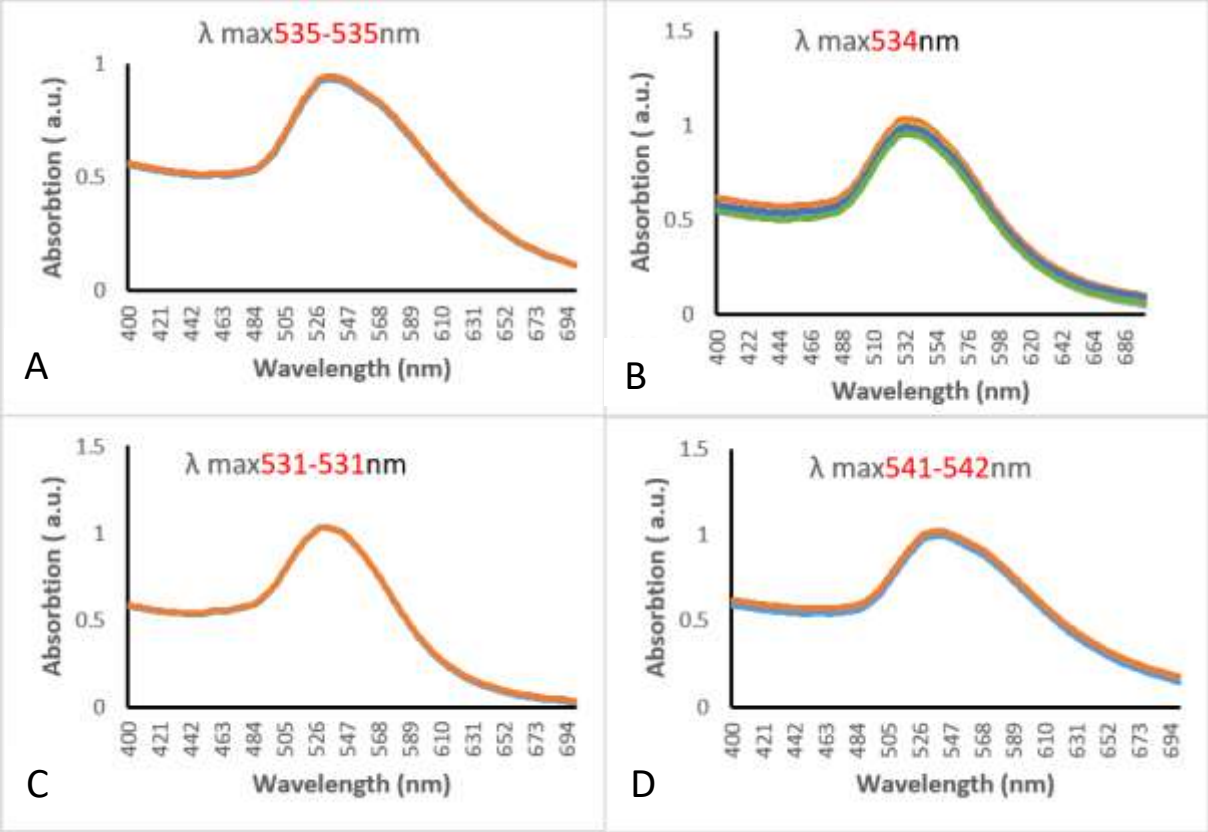

Figure 14. UV-Visible spectra for analyzed gold nanoparticles showing the position of surface plasmon resonance peak bands [λmax] for different batches (Batch5-A, batch6-B, batch7-C, batch8-D)

As presented, all batches available demonstrated λmax in the range of 531 to 535 [except batch 8; still no aggregations], which made them perfect candidates for following coating process.

8.4 UV-Vis spectrometry-based detection of LPEI-SH coating on gold NPs

During the coating Experiment 1, there was no aggregation noticed and the UV-Vis check provided 2 nm shift in the first experiment as shown in Figure 15.

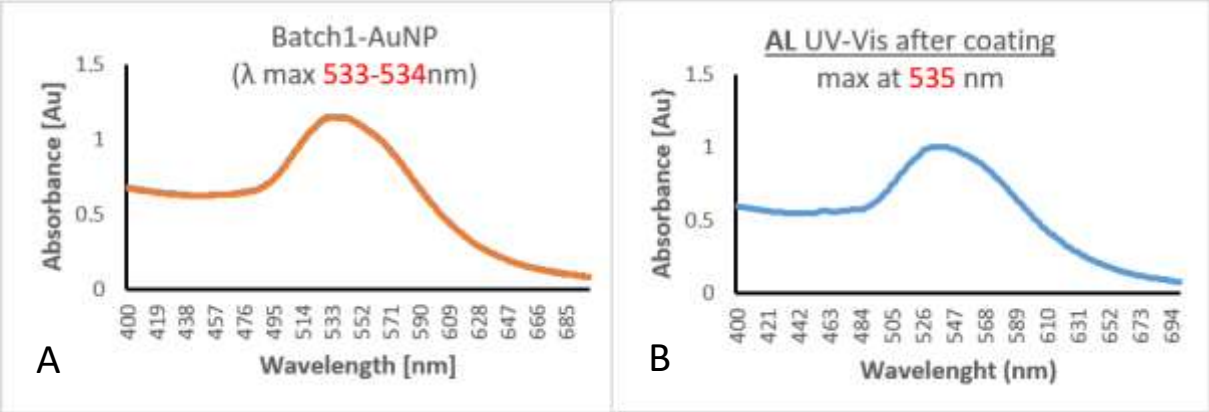

Figure 15. SPR shift before [A] and after coating [B]. Here presented are results from Experiment 1 using unpurified AL solution right after the coating process in the range of 400 to 700nm. Peak maximum labeled in red.

In the next coating experiment [Experiment 2], the formulation is the same, just scaled down [5038.2 µl of AuNP + 461.8 µl of LPEI]. Surprisingly, conjugates or ALs demonstrated this time a shift of 10 nm [Figure 16], which is in previous studies associated with successful functionalization.

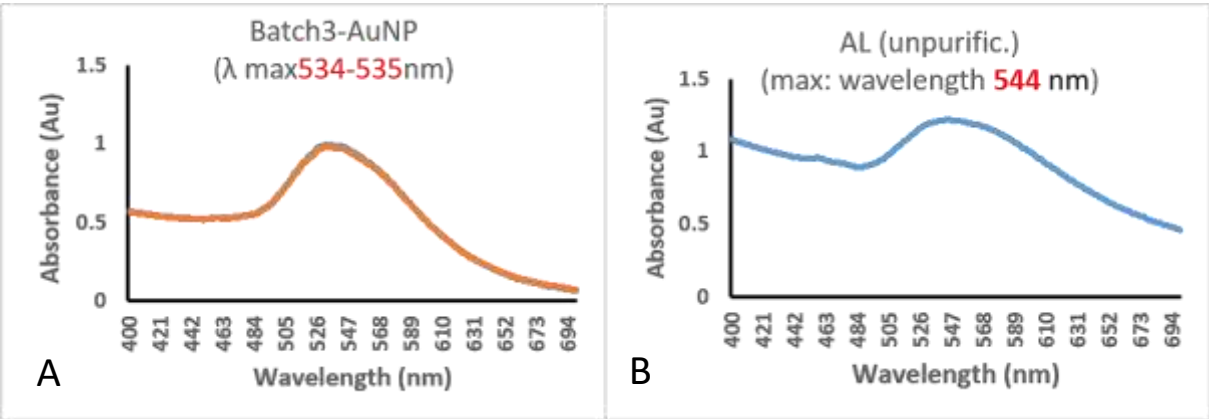

Figure 16. SPR shift before [A] and after coating [B]. Here presented are results from Experiment 2 using unpurified AL solution right after the coating process in the range of 400 to 700nm. Peak maximum labeled in red.

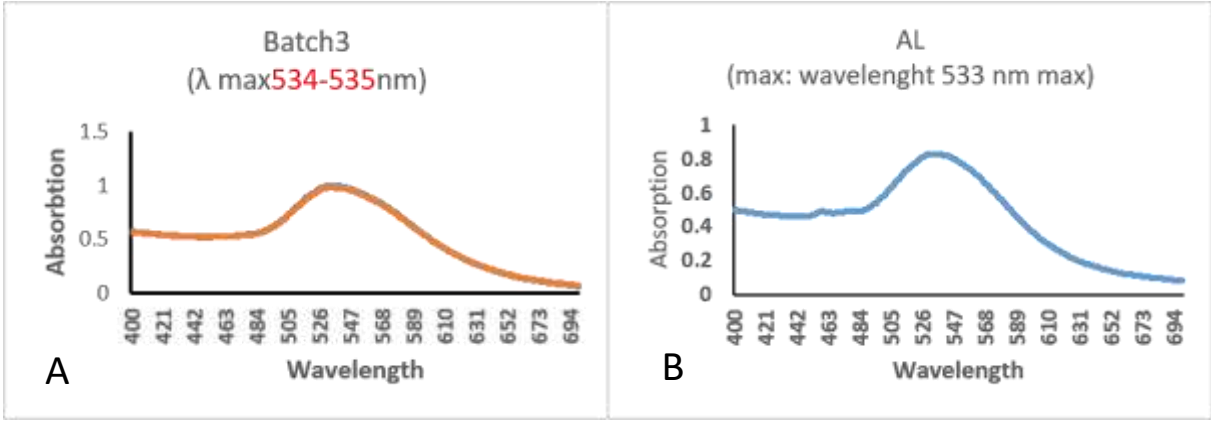

Figure 17. SPR shift before[A] and after coating[B]. Here presented are results from Experiment 3 using unpurified AL solution right after the coating process in the range of 400 to 700nm. Peak maximum labeled in red.

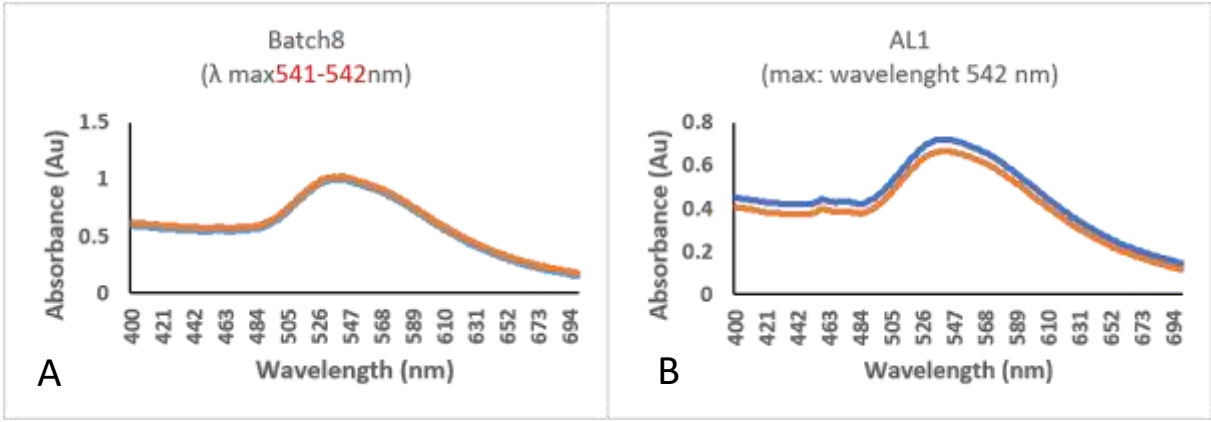

Figure 18. SPR shift before[A] and after coating [B]. Here presented are results from Experiment 4 using unpurified AL solution right after the coating process in the range of 400 to 700nm. Peak maximum labeled in red.

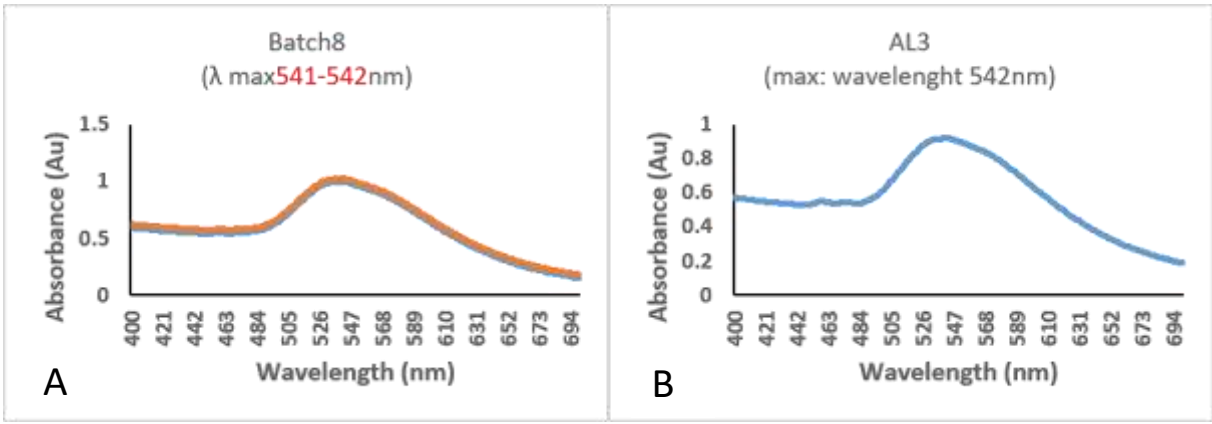

Figure 19. SPR shift before[A] and after coating[B]. Here presented are results from Experiment 5 using unpurified AL solution right after the coating process in the range of 400 to 700nm. Peak maximum labeled in red.

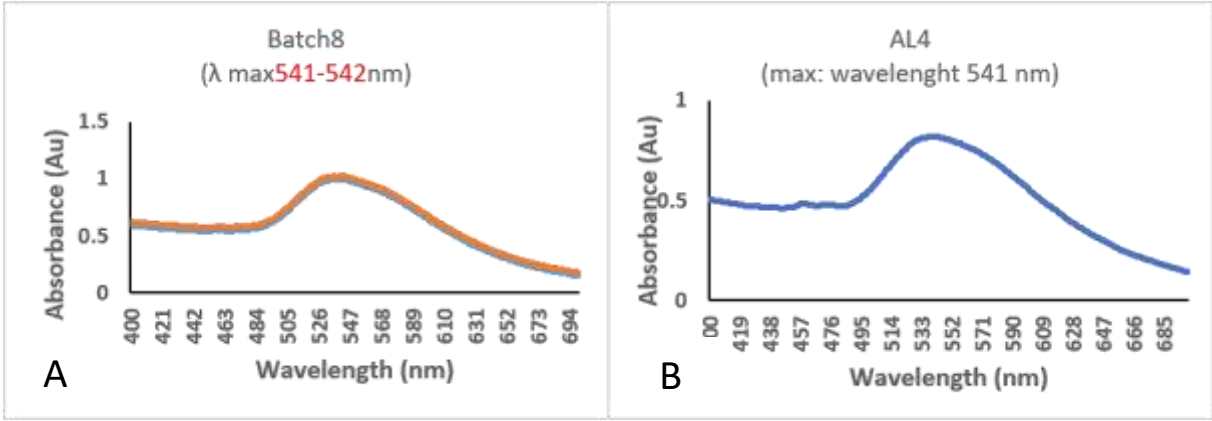

Figure 20. SPR shift before[A] and after coating[B]. Here presented are results from Experiment 6 using unpurified AL solution right after the coating process in the range of 400 to 700nm. Peak maximum labeled in red.

During the coating of Experiment 4,5 and 6 there was no aggregation noticed, but also the UV-Vis check provided only 1 to 2 nm shift as shown in Figure 18,19, and 20. In case of Experiment 3 there was no shift detected at all.

8.5 Indirect quantification

To test if shift correlates with the actual amount of LPEI bound on gold nanoparticles, indirect and direct quantifications of LPEI using Cu-assay have been conducted. But before that, all solutions were purified with extra caution, trying not to change the concentration of solutions by transferring NP in supernatants or washes. Table3 shows an overview of the results of the amount of LPEI on AL nanoparticles estimated by indirect quantification.

Experiment	Batch	AuNP volume used (ul)	LPEI-SH volume added for coating (ul)	UV-Vis SPR shift	Total LPEI added for coating	LPEI in super./ Washes (total)	LPEI on AL By INDIRECT QUANT in % (ug)
Experiment 1	1	10076.35 µl	923.65 µl	2 nm	12593 µg	11979 µg	**4.87%** (613.9 µg)
Experiment 2	3	5038.178 µl	461.825	10 nm	6296.9 µg	4606.8 µg	**26.8%** (1690.1 µg)
Experiment 3	7	2500 µl	461 µl	2 nm	6296 µg	6172 µg	1.9% (124 µg)
Experiment 4	8	2500 µl	923.65 µl	1 nm	12607.82 µg	1030.5 µg	18.2% (2303 µg)
Experiment 5	8	5000 µl	461 µl	1 nm	6296 µg	6350 µg	0 µg
Experiment 6	8	5000 µl	923.65 µl	0 nm	12607.82 µg	11849.4 µg	6% (758.4 µg)

Table 3. Experiment overview with results from indirect quantification of LPEI. The percentage of LPEI still bound on all successfully produced AL after 6 rounds of purification [highlighted in red].

The indirect quantification of the first coating [Experiment 1] resulted in a total of 11979 µg LPEI found in supernatants and washes, which makes it 4.8 % considering the total amount consumed [12593 µg]. Expressed differently, still 613.9 µg LPEI is on the gold surface. All values with dilutions rate, as well as calculations, are presented in Table 4.

	S1	S2	mean absorption	std. dev.	n	conc. dil (µg/ml)	dil. factor	end conc. (µg/ml)	ml end vol.	total amount excess LPEI (µg)
supernatant	1.256	1.256	1.256	0	2	117.8716	10	1178.716	9	10608.44
wash 1	0.664	0.651	0.6575	0.009192	2	62.9633	2	125.9266	9	1133.339
wash 2	0.226	0.213	0.2195	0.009192	2	22.77982	1	22.77982	9	205.0184
wash 3	0.008	0.015	0.0115	0.00495	2	3.697248	1	3.697248	9	33.27523
wash 4	0	0	0	0	2		1	0	9	0
Wash 5	0	0	0	0	2		1	0	3	0
Total:										11979

Table 4. Estimated values in supernatant and washes multiplied with particular dilutions; All washes and supernatant collected in purification process of Experiment 1 with the total amount of LPEI as a sum from each separately wash multiplied with end volume

In the case of Experiment 1, the results strongly indicate that more LPEI has been bound. Indirect quantification further revealed that 4606.8 µg LPEI is in supernatant/washes. Hence, the total amount of LPEI bound in percentage is 26.8% [presented in Table 6]. Knowing that the UV-Vis shift was 10 nm, this was expected. It is also important to notice that the total amount used this time was 6296.9 µg if we want to compare it with Experiment 1[see Table 6 for all values].

	S1	**S2**	**mean absorption**	**std. dev.**	**n**	**conc. dil (µg/ml)**	**dil. factor**	**end conc. (µg/ml)**	**ml end vol.**	**total amount excess LPEI (µg)**
supernatant	1.038	1.036	1.037	0.001	2	97.77982	10	977.7982	4	3911.193
wash 1	0.682	0.676	0.679	0.003	2	64.93578	2	129.8716	4	519.4862
wash 2	0.203	0.214	0.2085	0.0055	2	21.77064	1	21.77064	4	87.08257
wash 3	0.041	0.06	0.0505	0.0095	2	7.275229	1	7.275229	4	29.10092
wash 4	0.035	0.041	0.038	0.003	2	6.12844	1	6.12844	4	24.51376
wash 5	0.017	0.026	0.0215	0.0045	2	4.614679	1	4.614679	4	18.45872
wash 6	0.02	0.015	0.0175	0.0025	2	4.247706	1	4.247706	4	16.99083
Total:										4606.826

Table 5. Indirect quantification: estimated values in supernatant and washes multiplied with particular dilutions; All washes and supernatant collected in purification process of Experiment 2 with the total amount of LPEI as a sum from each separately wash multiplied with end volume

In accordance with the shift phenomena mentioned before, it was not surprising that in Experiment 2 more LPEI "stayed" on AuNPs in comparison with Experiment 1 [Table 7 shows comparison]. Since experimental conditions were the same in both Experiment

1 and Experiment 2, it is still not confirmed what led to different coating outcomes, not only in the case of Experiment 2 but also in all the following experiments.

	The total amount of LPEI used for coating	**LPEI in supernat./ washes**	**LPEI on AL by INDIRECT QUANT (ug)**	**LPEI on AL by INDIRECT QUANT (%) Percent of total LPEI added**
Exp.1	6296.9 µg	4606.8 µg	1690.1 µg	**26.8%** of added got bound to AL
Exp.2	12593 µg	11979 µg	613.9 µg	**4.87%** of added got bound to AL

Table 6. Comparison of indirect quantification: Experiment 1 vs Experiment 2. Measurement conditions, in order to obtain reproducibility of data, kept the same for both experiments.

Interestingly, after Experiment 2 there was no coating done with shift bigger than 2 nm retrospectively [Table 9 with failed experiments can be found in appendix]. Subsequently, the LPEI loads found in further attempts using the indirect method, which ranged from 1.9 to 18.2%, conformed correlation from the previous example in Experiment 1/Experiment 2.

Additionally, tables with calculations of all indirect quantifications [Tables 11-15] can be found in the appendix.

8.6 Direct quantification of LPEI

Table7 shows an overview of results of amount of LPEI on AL nanoparticles estimated by direct quantification for the same set of experiments as presented for indirect quantification.

	AuNP volume used (ul)	**LPEI-SH volume added for coating (ul)**	**UV-Vis SPR shift**	**Total LPEI added for coating**	**LPEI in super./ Washes (total)**	**LPEI on AL By INDIRECT QUANT in % (ug)**	**LPEI on AL by DIRECT QUANT in % (ug)**
Exp.1	10076.35 µl	923.65 µl	2 nm	12593 µg	11979 µg	4.87% (613.9 µg)	**0.59%** (26.29 µg)
Exp.2	5038.178 µl	461.825	10 nm	6296.9 µg	4606.826 µg	26.8% (1690.1 µg)	**8.7%** (547.7 µg)
Exp.3	2500 µl	461 µl	2 nm	6296 µg	6172 µg	1.9% (124 µg)	0.11% (7.3µg)
Exp.4	2500 µl	923.65 µl	1 nm	12607.82 µg	10304.5 µg	18.2% (2303 µg)	0.04% (4.9µg)
Exp.5	5000 µl	461 µl	1 nm	6296 µg	6350 µg	0 µg	0.13% (8.5µg)
Exp.6	5000 µl	923.65 µl	0 nm	12607.82 g	11849.4 µg	6% (758 µg)	-

Table 7. Experiments overview with final calculations [in red] from direct quantification of LPEI. In the same row included are all related information necessary for quick comparison between all successfully experiments including formulations, SPR shift, and final quantification outcomes presented in percentage.

Before direct quantification of LPEI on AL nanoparticles was performed, we studied the difference in absorption of different dilutions of coated AL NPs (via Cu assays) Since too concentrated or too diluted AL solution could not be used due to absorption limitation, the estimation of the detectible window was needed [example of 3 different dilutions presented in the following figure]. Although, it varied from experiment to experiment, at least one example is presented in Figure 21.

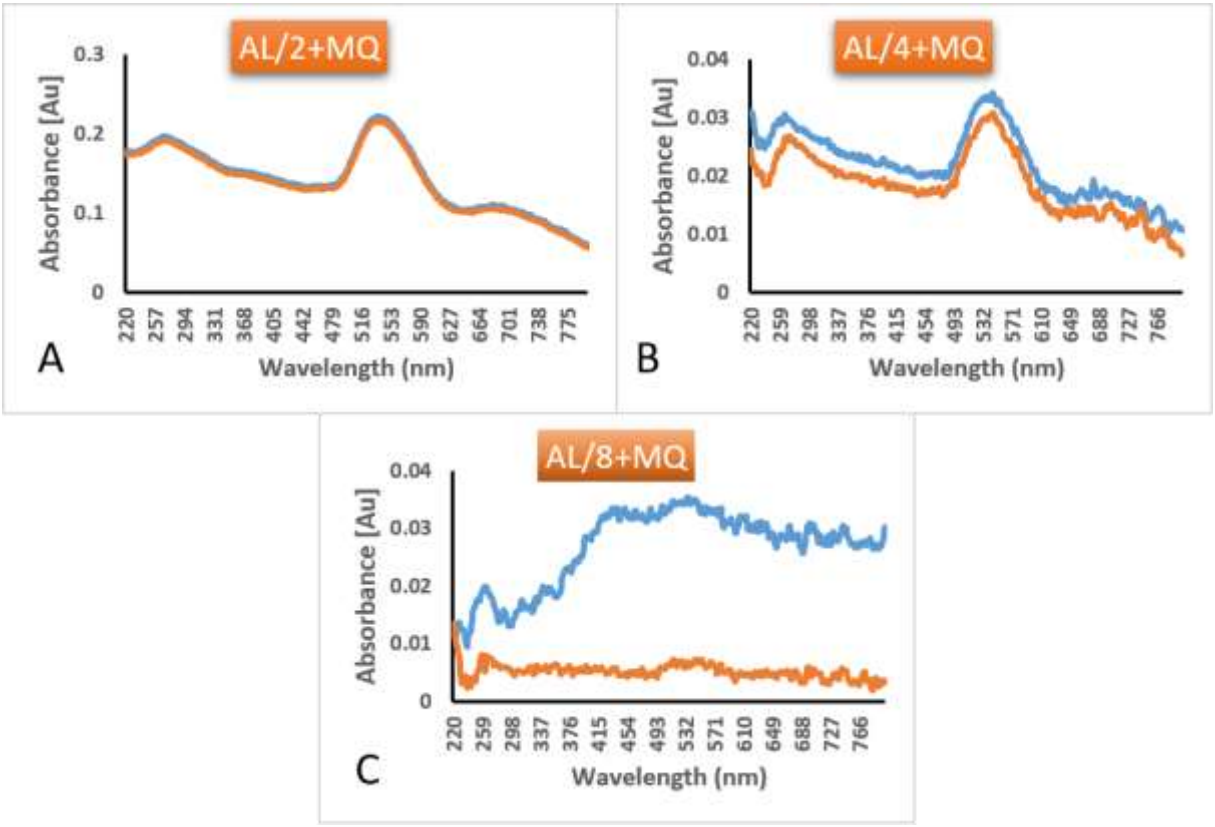

Figure 21. Comparison of different dilution factors of AL by measuring UV-Vis spectra. As presented, there is an enormous difference comparing 1 to 2 dilution [A] of purified AL with MiliQ, 1 to 4 [B], and 1 to 8 [C].

The next step was direct quantification or quantification directly on AL particles [the detailed procedure provided in the Material and methods section] using the same

principle utilized in indirect. For this purpose, only selected dilutions can be included in final calculations due to diverse concentration rates which are highly dependent on formulations and purification work. Table 8 displays an estimation of LPEI direct, just as an example, in two separate experiments where relevant dilutions are presented in green color [to follow experiment values, understanding of the method and blanks unnecessary]. In brief, 'green' values are used for the final calculation of LPEI amount as the average from few dilutions [for instance, in Experiment 3 only one could be considered; this altogether must be taken into account when discussing].

	AL/40	AL/80	AL/160
Absorption double blanked	1.377583	0.705433	0.371833
Absorption of AL+Cu	2.33	1.2311	0.687833
Absorption of Cu+MQ	0.135167	0.135167	0.135167
Absorption AL+MQ	0.81725	0.3905	0.180833

concentration LPEI (µg/ml)	**129.03**	**67.36**	**36.76**
dilution factor	**40**	**80**	**160**
concentration LPEI (µg/ml) final	**5161.04**	**5388.87**	**5880.85**
concentration LPEI (µg/ml) stock	5161.04	5388.87	5880.85
amount LPEI in stock total (µg)	516.10	538.89	588.09
Average:	**547.69**		

	AL/5	AL/10	AL/20	AL/40
Absorption double blanked	-0.091	-0.0125	0.011	-0.0065
Absorption of AL+Cu	1.176	0.7415	0.4165	0.2605
Absorption of Cu+MQ	0.135	0.135	0.135	0.135
Absorption AL+MQ	1.132	0.619	0.2705	0.132

concentration LPEI (µg/ml)	**-5.71**	**1.50**	**3.65**	**2.05**
dilution factor	**5**	**10**	**20**	**40**
concentration LPEI (µg/ml) final	**-28.53**	**14.95**	**73.03**	**81.83**
concentration LPEI (µg/ml) stock	-28.53	14.95	73.03	81.83
amount LPEI in stock total (µg)	-2.85	1.50	**7.30**	8.18

Table 8. Overview of parameters and suitable dilution rates. Here presented are two experiments [above: Experiment 2; below: Experiment 3] in the purpose of quantitative estimation of LPEI on AL.

Tables with calculations of all direct quantifications can be found in the appendix [Tables 16-19]. And now, to investigate the reliability and validity of data, by simply comparing final estimations in both methods [see Table 7] it is obvious that they vary relatively much. However, it is also clearly evident that only in the case of Experiment 2 [SPR shift here was 10 nm!] notably greater amount of LPEI could be evaluated. This indicates successful coating of gold nanoparticles with LPEI-SH in case of Experiment 2 and thus this batch of purified cationic AL nanoparticles were used for testing their potential of SSO complexation in the next goal of the thesis.

8.7 Complexation of SSO with purified cationic gold nanoparticles (AL)

Since coating and purification in the case of Experiment 2 showed promising results, indicating no aggregation, it was continued in the next phase: one-step complexation of AL [AL yield from Experiment 2] with SSO. The aim of this experiment was to test the functionality of AL by bounding and detecting SSO on it using gel electrophoresis.

The optimum amount of SSO for gel retardation studies was first estimated. Toward this end, concentrations ranging from 200 to 600 ng of SSO were chosen and detection in the gel was examined using ChemiDoc MP Imaging System [Figure 22]. Our results revealed that 300 ng of SSO is certainly enough for successful imaging and exactly this concentration will be used for imaging of further one-step complexation experiments.

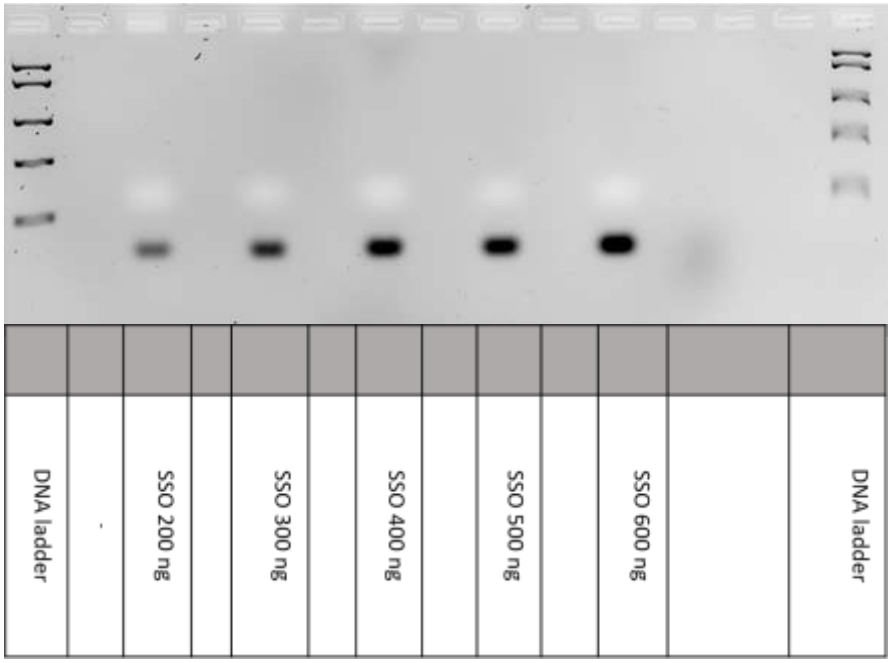

Figure 22. Detection of optimal SSO amount for best visualization in gel electrophoresis. Here pure SSO was used in different concentrations for this purpose. For each loading, the same volume inserted independently of concentration [electrophoresis was done at 80 V; agarose 1.5% gel imaged directly after 32 minutes of running].

And yet, for purpose of complexation of SSO with AL, the same technique used for polyplexing was employed here [see Polyplexing section in Material and methods for more information], or so-called flash-pipetting. After purification AL-Experiment 2 end volume was concentrated to 100 µL and from this stock different dilutions were made and used in gel retardation, so this must be taken into account along with the formulation. It needs to be pointed out that for all experiments, complexations worked in a single step with great reproducibility containing 300 ng of AF 750 SSO for each complex. To observe the behavior of those, gel electrophoresis imaging has been performed twice: after 12 minutes [Figure 23] and after 32 minutes of running [Figure 24]. Finally, all AL dilutions [from 100 µL stock after purification of AL Experiment 2]

up to 1:1600 were able to complex 300 ng of SSO. In other words, these results (presented below) illustrated that very low amounts of AL are needed for the complete retardation of SSO in a single complexation step.

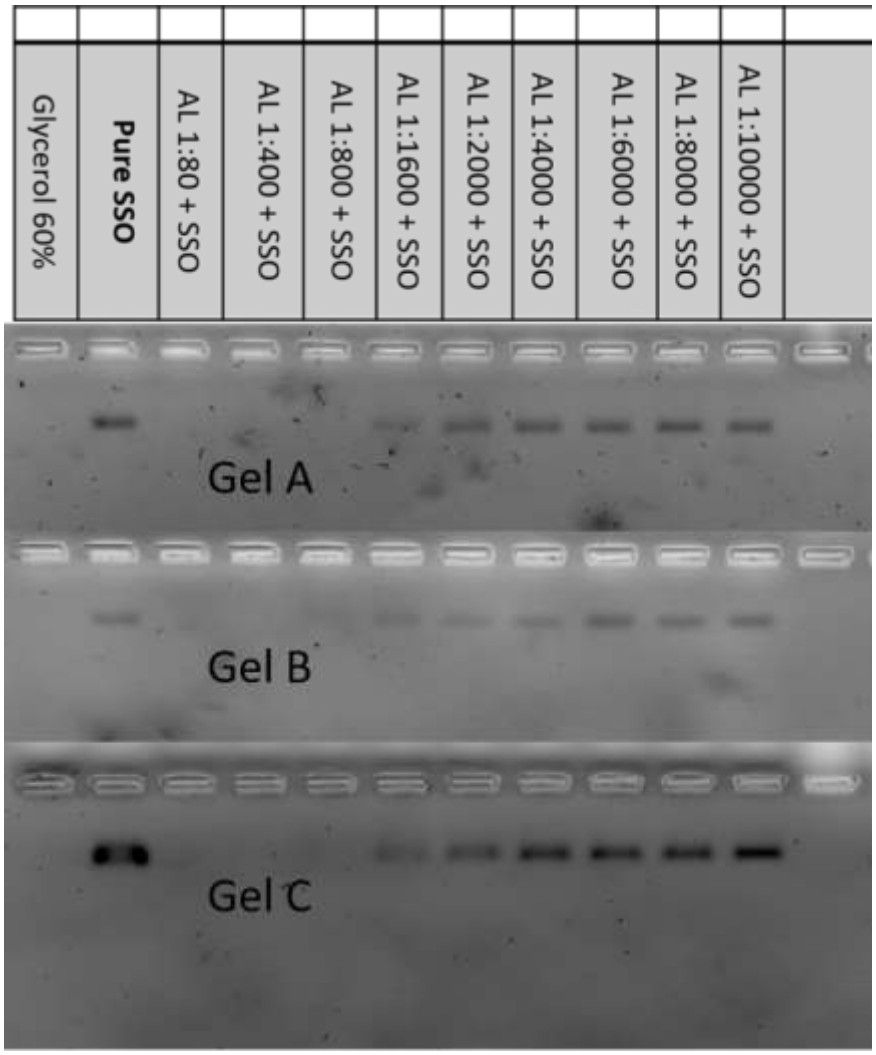

Figure 23. Gel retardation of AL + SSO complexation. All 3 gels were prepared under the same conditions [electrophoresis was done at 80 V; agarose 1.5% gel imaged directly after 12 minutes of running]. For this single-step complexation only purified AL from Experiment 2 was examined.

All supplementary gel images associated with one-step complexation of SSO with AL can be found in the appendix.

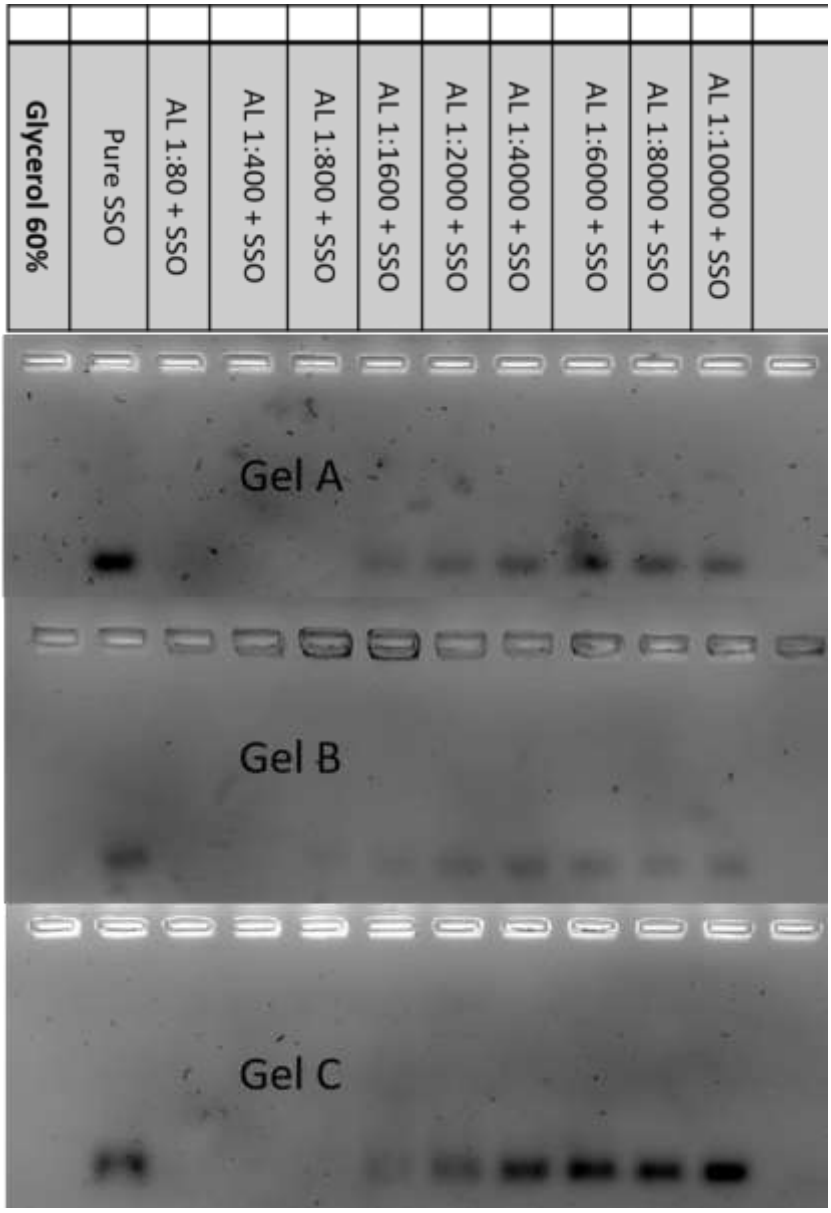

F**igure 24**. Gel retardation of AL + SSO complexation. All 3 gels were prepared under the same conditions [electrophoresis was done at 80 V; agarose 1.5% gel imaged directly after 32 minutes of running]. For this single-step complexation only purified AL from Experiment 2 was examined.

We attribute this significant complexation rate between AL and SSO to a high concentration of cationic nanoparticles (with LPEI-SH bound on their surface) in solution after purification but also to the successful coating which preceded it. This is supported by the high amount of LPEI-SH on the AL nanoparticles as estimated by indirect and direct quantification.

8.8 Polyplexing of siRNA with PEI

8.8.1 siRNA/LPEI polyplexes

The main aim of this project was to determine in which proportion siRNA will be complexed with LPEI with respect to incubation time and compare the complexation pattern of linear vs branched versions of PEI. The procedure of polyplexing and flash-pipetting has been detailed explained in the Material and methods section. In brief, it is been revealed that from the N/P 3 ratio onwards all siRNA will be complexed and there is no difference evident between 0 and 30 minutes incubation time as presented in Figure 19. For each experiment, we used 1.5 % agarose gel and the voltage was set on 100V for 45 minutes. In order to archive reproducibility, there were in total 3 gels for each 0 min incubation- and 30 min incubation time produced, loaded, imaged and analyzed.

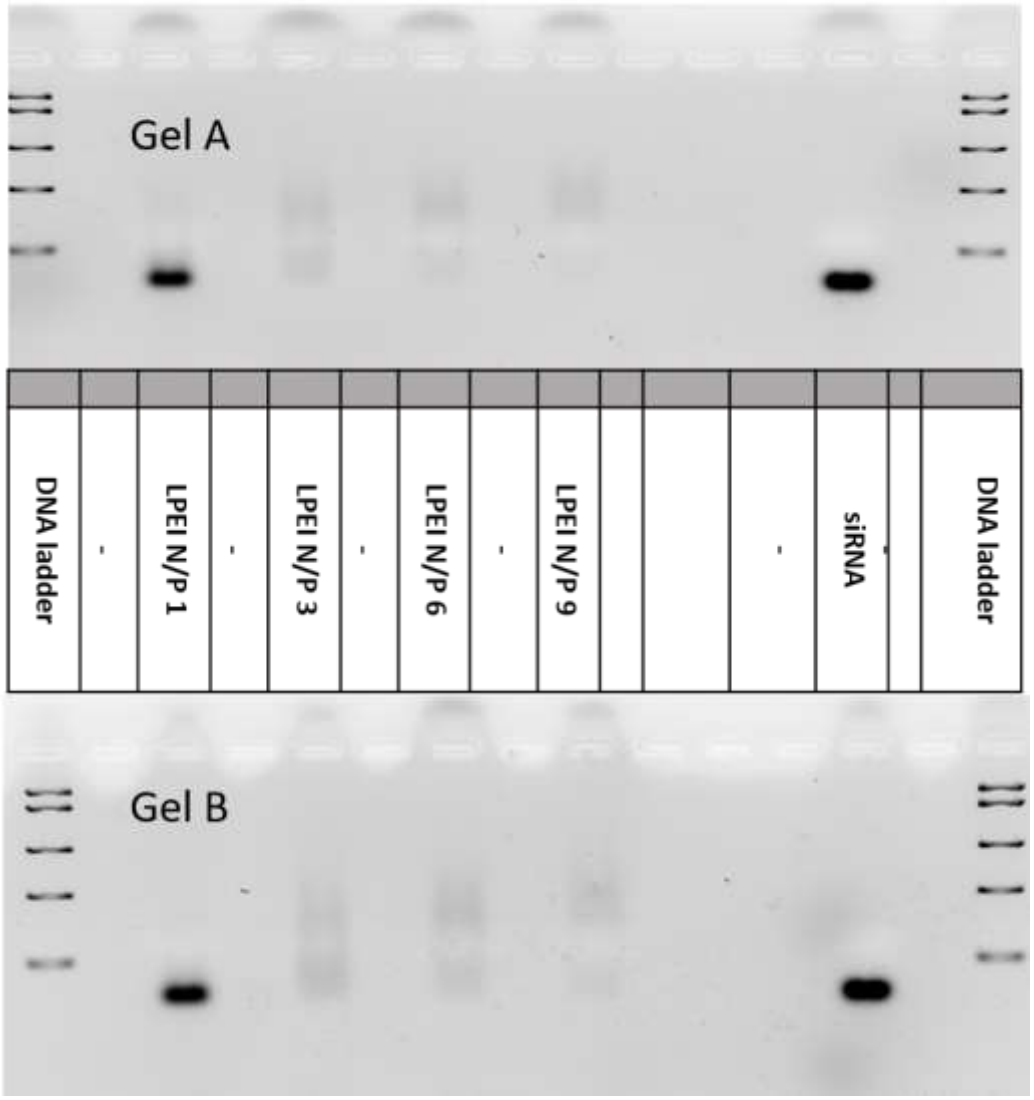

Figure 25. Gel retardation of siRNA/LPEI complex. Different N/P ration [1,3,6,9] were tested; above [Gel A]: no incubation time vs below [Gel B]: 30 min incubation time on room temperature [electrophoresis was done at 100 V; agarose 1.5% gel imaged directly after 45 minutes of running].

8.8.2 siRNA/BPEI polyplexes

This experiment shares exactly the same parameters setup as the previous one with siRNA/LPEI. In summary, the results [Figure 20] depict no difference from results obtained for LPEI complexation considering incubation time and N/P ratio.

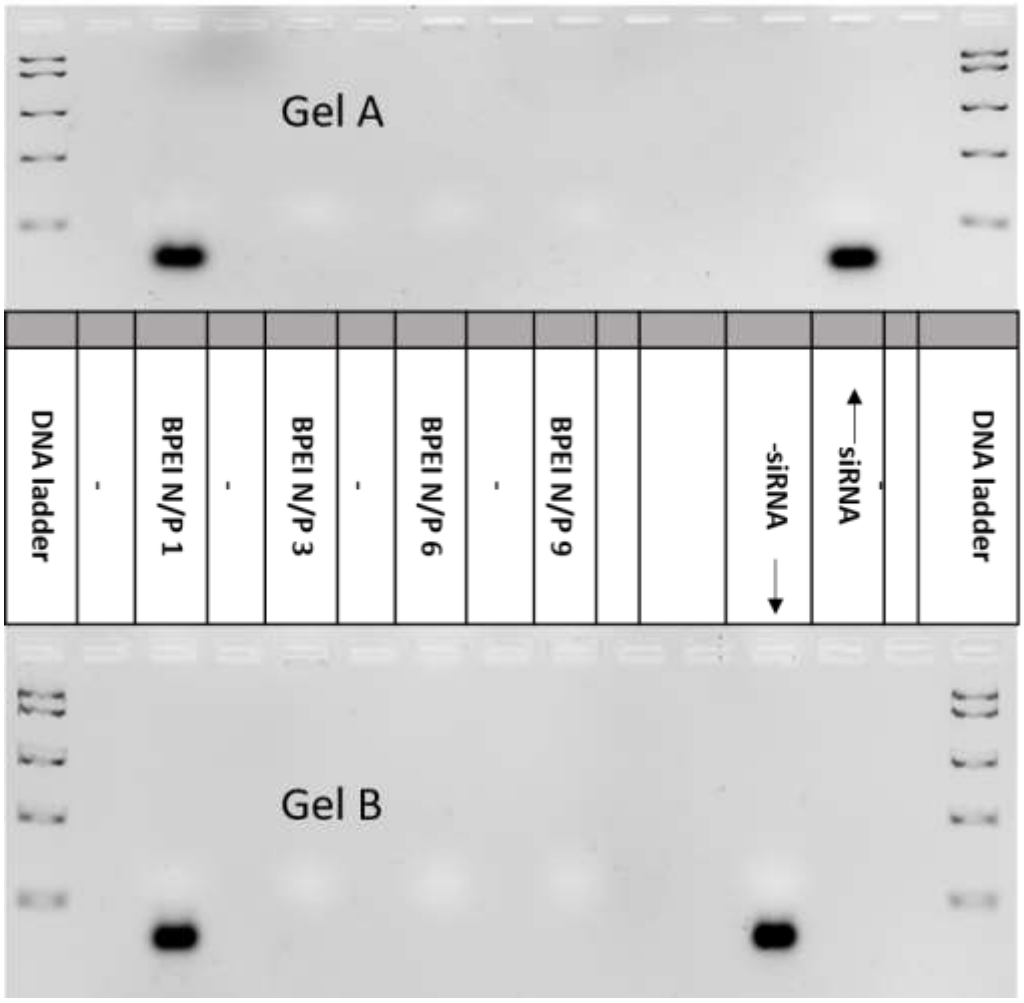

Figure 26. Gel retardation of siRNA/BPEI complex. Different N/P ration [1,3,6,9] were tested; above [Gel A]: no incubation time vs below [Gel B]: 30 min incubation time on room temperature [electrophoresis was done at 100 V; agarose 1.5% gel imaged directly after 45 minutes of running].

In summary, considering measurement conditions, formulations, and all facts relative to the complexation rate between polyethyleneimine and siRNA, to the best of our knowledge, there is no difference observed in polyplexing in either LPEI or BPEI case if N/P ratio stays the same. The process and results cannot be affected by longer incubation time [30min].

9. Conclusion and Outlook

Since biodistribution of gene cargo is a crucial factor for gene therapy, auropolyplexes can offer a novel form of gene vehicles with high binding affinity and relatively uncomplicated manufacture. In this thesis, colloidal gold nanoparticles have been investigated as a small but important model of possible hybrid materials.

Because the process of coating of gold with PEI is still not established but based on the already accepted knowledge of auropolyplexes it is been continued with optimizing applicable methods to produce these. More fundamentally, detailed biophysical characterizations were conducted and analyzed with a focus on quantification of PEI needed for optimal coating. Therefore, various formulations were tested in order to generate homogeneity and particles resistant to aggregation. Unfortunately, we are still not able to confirm reproducibility in the production of AL [coating of gold NP] due to an insufficient number of successful experiments. But to realize the exceptional potential of Au conjugates it is essential to report the results from Experiment 2. Here, in accordance with the phenomena reported in the literature, it is evident how quickly coated gold nanoparticles with optimal red-shifted properties and high yield can be prepared. It is therefore unsurprising that the same NPs provided an excellent model for complexation even in small amounts. Working with this sample, it was observed that the purified AL NP sample is stable for more than 6 weeks, which is characterized as greatly enhanced stability relative to their former counterparts. Hence, our results show a good correlation between SPR shift and LPEI bound on AL by indirect and direct quantification methods. Furthermore, it is obvious that complexation with all reproducibility is available only if the coating was successful. But since all data was gathered from a single experiment, subsequently, these findings need further investigations for establishing the reproducibility.

The next aim of this thesis was to estimate the LPEI load spent in the coating phase of AuNP. It is hoped that eventual understanding of this mechanism and LPEI costs can be employed to enhance more effective auropolyplex-mediated gene biodistribution. The quantification itself was established on the current, widely-used Copper assay. To provide the most accurate assessment of LPEI bound on AuNPs, correspondence between indirect and direct method has been provided. In summary, as results have been demonstrated, there has not been a significant parallel up to now, in both indirect and direct quantification of LPEI, considering LPEI payload and LPEI amounts found using a Copper assay as quantification approach. Since this work lacks more coatings with a shift greater than 1-2 nm as well as an enormous distinction in final values considering indirect and direct quantification comparatively, it was not possible to establish a direct interrelationship between these two methods.

In future work, efforts need to be devoted to constructing the AL with different parameters under diverse conditions in order to achieve efficiency in gene delivery.

The second part of this work was devoted to calculate and test an adequate proportion of PEI to siRNA considering the number of nitrogen and phosphate atoms. Besides the N/P ratio, the incubation time was taken into account. Our findings demonstrate that N/P ratio 3 is required to achieve a 100% complexation rate, in both LPEI and BPEI samples. Additional, we observed that there is no difference between 30 minutes of incubation time and no incubation time at all.

10. Appendix

List of failed experiments within auropolyplex project:

	Batch	AuNP volume used (ul)	LPEI-SH volume added for coating (ul)	
P1.2 (AL 1)	3	10079.35	923.65	**ALL AGGREGATED IMMEDIATELY**
P1.2 (AL3)	3	5038.17	230.91	
P1.3	7	5038.175	461.825	
P1.4 (AL1)	7	5038.175	1 drop of LPEI	
P1.4 (AL2)	7	5038.175	1 drop of LPEI	
P1.4 (AL3)	7	5038.175	20µl of LPEI	
P1.5 (AL2)	8	2500	923.65	

Table 9. Formulation of the experiments which aggregated during the coating process.

		Absorption	Wavelength(nm)
Batch1	Measurement 1	1.15045	533
	Measurement 2	1.14389	534
Batch2	Measurement 1	1.0646	534
	Measurement 2	1.04147	535
Batch3	Measurement 1	0.993016	534
	Measurement 2	0.978447	535
Batch4	Measurement 1	1.01622	535
	Measurement 2	0.986802	535
Batch5	Measurement 1	0.934073	535
	Measurement 2	0.946041	535
Batch6	Measurement 1	0.98447	532
	Measurement 2	1.03282	532
	Measurement 3	0.971685	534
	Measurement 4	1.00125	533
	Measurement 5	0.989448	534
	Measurement 6	0.95342	534
Batch7	Measurement 1	1.03355	531
	Measurement 2	1.03131	531
Batch8	Measurement 1	0.992468	541
	Measurement 2	1.02191	542
Batch9	Measurement 1	1.02603	532
	Measurement 2	1.02028	532

Table 10. The summary of nine absorption measurements with SPR maxima

10.1 Indirect quantification results

	S1	S2	mean absorption	std. dev.	n	conc. dil (µg/ml)	dil. factor	end conc. (µg/ml)	ml endvol.	total amount excess LPEI (µg)
Supernat.	2.293	2.302	2.2975	0.0045	2	213	10	2134.22	2.5	5335.55
wash 1	1.442	1.378	1.41	0.032	2	132	2	264.00	2.5	660.00
wash 2	0.436	0.448	0.442	0.006	2	43	1	43.19	2.5	107.98
wash 3	0.166	0.156	0.161	0.005	2	17	1	17.41	2.5	43.53
wash 4	0.038	0.028	0.033	0.005	2	6	1	5.67	2.5	14.17
wash 5	0	0	0	0	0	3	1	2.64	2.5	6.61
wash 6	0.02	0.018	0.019	0.001	2	4	1	4.39	1	4.39
									Total:	**6172.23**

Table 11. Indirect quantification: estimated values in the supernatant and washes multiplied with particular dilutions; Experiment 3 (AL 4)

	S1	S2	mean absorption	std. dev.	n	conc. dil (µg/ml)	dil. factor	end conc. (µg/ml)	ml endvol.	total amount excess LPEI (µg)
Supernat.	1.924	1.902	1.913	0.011	2	178	20	3562.94	2.5	8907.34
wash 1	1.81	1.833	1.8215	0.0115	2	170	2	339.50	2.5	848.76
wash 2	1.788	1.803	1.7955	0.0075	2	167	1	167.37	2.5	418.42
wash 3	0.317	0.35	0.3335	0.0165	2	33	1	33.24	2.5	83.10
wash 4	0.134	0.111	0.1225	0.0115	2	14	1	13.88	2.5	34.70
wash 5	0	0	0	0	0	3	1	2.64	2.5	6.61
wash 6	0.03	0.034	0.032	0.002	2	6	1	5.58	1	5.58
									Total:	**10304.50**

Table 12. Indirect quantification: estimated values in the supernatant and washes multiplied with particular dilutions; Experiment 4 (AL1)

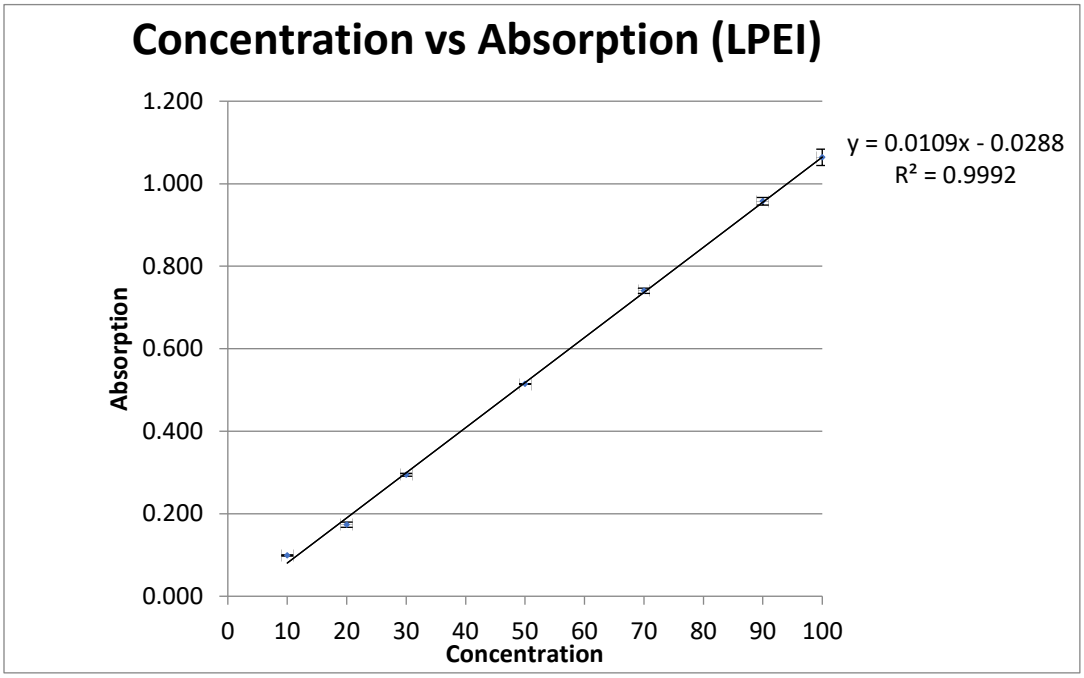

Figure 26. The standard curve used for indirect quantification of LPEI. At the upper right corner presented is formula utilized for final calculations [based on standard curve calculations in excel]. Figure from reference (Decker, 2019)

conc. (µg/ml)	Absorption S1	Absorption S2	Absorption (average)	std. dev.
10	0.098	0.100	0.099	0.00141
20	0.178	0.169	0.174	0.00636
30	0.297	0.292	0.295	0.00354
50	0.515	0.514	0.515	0.00071
70	0.745	0.736	0.741	0.00636
90	0.951	0.964	0.958	0.00919
100	1.078	1.050	1.064	0.01980

Table 13. The standard curve copper assay values. For this purpose, different concentrations [10 to 100 µg/ml] were produced using LPEI 22 kDa [unfiltered], CuSO4 solution labeled under 151118 SD. Table from reference (Decker, 2019)

	S1	S2	mean absorption	std. dev.	n	conc. dil (µg/ml)	dil. factor	end conc. (µg/ml)	ml endvol.	total amount excess LPEI (µg)
Supernat.	1.225	1.221	1.223	0.002	2	115	10	1148.44	4.5	5167.98
wash 1	1.011	1.021	1.016	0.005	2	96	2	191.71	4.5	862.68
wash 2	0.483	0.501	0.492	0.009	2	48	1	47.78	4.5	215.01
wash 3	0.113	0.142	0.1275	0.0145	2	14	1	14.34	4.5	64.53
wash 4	0.038	0.041	0.0395	0.0015	2	6	1	6.27	4.5	28.20
wash 5	0	0	0	0	0	3	1	2.64	4.5	11.89
wash 6	0.029	0.018	0.0235	0.0055	2	5	1	4.80	0.0034	0.02
									Total:	**6350.30**

Table 14. Indirect quantification: estimated values in the supernatant and washes multiplied with particular dilutions; Experiment 5

	S1	S2	mean absorption	std. dev.	n	conc. dil (µg/ml)	dil. factor	end conc. (µg/ml)	ml endvol.	total amount excess LPEI (µg)
Supernat.	2.266	2.277	2.2715	0.0055	2	211	10	2110.37	4.5	9496.65
wash 1	1.81	1.849	1.8295	0.0195	2	170	2	340.97	4.5	1534.38
wash 2	1.394	1.402	1.398	0.004	2	131	1	130.90	4.5	589.05
wash 3	0.305	0.312	0.3085	0.0035	2	31	1	30.94	4.5	139.25
wash 4	0.154	0.167	0.1605	0.0065	2	17	1	17.37	4.5	78.15
wash 5	0	0	0	0	0	3	1	2.64	4.5	11.89
wash 6	0.027	0.044	0.0355	0.0085	2	6	1	5.90	0.0034	0.02
									Total:	**11849.39**

Table 15. Indirect quantification of Experiment 7. Estimated values in the supernatant and washes multiplied with particular dilutions;

10.2 Direct quantification results

wavelength (nm)	285			
volume stock (ml)	0.1	total after purific.		
the volume is taken from stock (µl)	25			
	AL/5	AL/10	AL/20	AL/40
Absorption double blanked	0.1	0.0145	-0.026	0.0145
Absorption of AL+Cu	1.5705	0.6635	0.351	0.179
Absorption of Cu+MQ	0.135	0.135	0.135	0.135
Absorption AL+MQ	1.3355	0.514	0.242	0.0295
concentration LPEI (µg/ml)	**11.82**	**3.97**	**0.26**	**3.97**
dilution factor	**5**	**10**	**20**	**40**
concentration LPEI (µg/ml) final	**59.08**	**39.72**	**5.14**	**158.90**
concentration LPEI (µg/ml) stock	59.08	39.72	5.14	158.90
amount LPEI in stock total (µg)	5.91	3.97	**0.51**	15.89
Average:	**4.94**			

Table 16. Direct quantification: estimated values found on AL multiplied with particular dilutions; Experiment 1

wavelength (nm)	285			
volume stock (ml)	0.25	total after purific.		
the volume is taken from stock (µl)	50			
	AL	AL/2	AL/4	AL/8
Absorption double blanked	-0.418489	0.085834	-0.078152	-0.169242
Absorption of AL+Cu	1.4329	0.628237	0.303594	0.196046
Absorption of Cu+MQ	0.355174	0.355174	0.355174	0.355174
Absorption AL+MQ	1.496215	0.187229	0.026572	0.010114
concentration LPEI (µg/ml)	**-35.75**	**10.52**	**-4.53**	**-12.88**
dilution factor	**1**	**2**	**4**	**8**
concentration LPEI (µg/ml) final	**-35.75**	**21.03**	**-18.11**	**-103.08**
concentration LPEI (µg/ml) stock	-35.75	21.03	-18.11	-103.08
amount LPEI in stock total (µg)	-8.94	5.26	-4.53	-25.77

Table 17. Direct quantification: estimated values found on AL multiplied with particular dilutions; Experiment 4

wavelength (nm)	285			

volume stock (ml)	0.1	total after purific.		
volume taken from stock (µl)	25			
	AL/5	AL/10	AL/20	Absorption was too low
Absorption double blanked	-0.501	0.023	0.0385	
Absorption of AL+Cu	0.8535	0.4365	0.2255	
Absorption of Cu+MQ	0.135	0.135	0.135	
Absorption AL+MQ	1.2195	0.2785	0.052	
concentration LPEI (µg/ml)	**-43.32**	**4.75**	**6.17**	
dilution factor	**5**	**10**	**20**	
concentration LPEI (µg/ml) final	**-216.61**	**47.52**	**123.49**	
concentration LPEI (µg/ml) stock	-216.61	47.52	123.49	
amount LPEI in stock total (µg)	-21.66	**4.75**	**12.35**	
Average:	**8.55**			

Table 18. Direct quantification: estimated values found on AL multiplied with particular dilutions; Experiment 5

wavelength (nm)	285			
volume stock (ml)	0.1	total after purific.		
volume taken from stock (µl)	25			
	AL/5	AL/10	AL/20	AL/40
Absorption double blanked	-0.68	-0.301	-0.087	-0.011
Absorption of AL+Cu	1.0145	0.557	0.336	0.174
Absorption of Cu+MQ	0.135	0.135	0.135	0.135
Absorption AL+MQ	1.5595	0.723	0.288	0.05
concentration LPEI (µg/ml)	**-59.74**	**-24.97**	**-5.34**	**1.63**
dilution factor	**5**	**10**	**20**	**40**
concentration LPEI (µg/ml) final	**-298.72**	**-249.72**	**-106.79**	**65.32**
concentration LPEI (µg/ml) stock	-298.72	-249.72	-106.79	65.32
amount LPEI in stock total (µg)	-29.87	-24.97	**-**10.68	6.53
Average:	**-27.42**			

Table 19. Direct quantification: estimated values found on AL multiplied with particular dilutions; Experiment 6

11.Feb.19												
P1- NC siRNA + LPEI25k- NP3; in HBS;								~~5picomol siRNA per well~~	~~1picomol siRNA = 0.01385 ug~~	~~5~~	~~0,06925~~	
Px2												
		Needed amount of siRNA										
	Final siRNA conc (ug/ml)	Np ratio	Amount of siRNA needed per well (ug)	No of total wells needed +1 bk up	Total siRNA needed (ug)	Volume in ml to be used for dispersing siRNA to maintain 4ug/ml	Volume in ul to be used for dispersing pDNA to maintain 4ug/ml		**Volume of nucleic acid needed from stock to take out required amount (ul)**	**Volume of HBS needed to make up polyplexing volume (ul)**		**total volume of NA in HBS for polyplexing (ul)**
	20	3	0,2	2	0,4	0,01	10		**4,00**	**6,00**		**10,00**
make siRNA stock of 100ug/ml by taking 2ul of 10000ug/ml stock + 198ul HBS	siRNA conc of stock in (ug/ml)	Amount of siRNA needed (ug)	Volume of siRNA needed from stock to take out required amount (ul)		~~Amount of siRNA needed (picomoles)~~							
	100	0,4	4,00		~~10~~							
		Needed amount of PEI										
make PEI stock of 100ug/ml by taking 10ul of 2827ug/ml stock + 272.7ul HBS	Nucleic acid amount (in total; in ug)	N/P ratio	Needed PEI amount (in ug)	^	**Vol of PEI needed from stock in ul**	**Vol of HBS to be added to make up to the required volume**	**total volume of PEI solution for polyplexing**					
	0,4	3	0,15	100	**1,52**	**8,48**	**10,00**					
		Polyplexing and addition to wells										
	total volume of NA for polyplexing (ul)	total volume of PEI solution for polyplexing (ul)										
	10,00	10,00										
								Vol (ul)				
	1. Add polymer to siRNA and mix by flash pipetting to get polyplexe							**20,00**				
	2. Add tjis 20ul polyplex to 4ul of laoding dye and load onto the well											

Table 20. Am example of calculating optimal N/P ratio for polyplexing of siRNA with LPEI and BPEI

AuNP-MR	Peak 1 (average diameter)	Peak 1 AUC (%)	Peak 2 (average diameter)	Peak 2 AUC (%)	PDL
1. Measurement	47,99	89,5 %	517,7	7,1 %	0,351
2. Measurement	52,47	82,6%	1496	14,4%	0,485
3. Measurement	48,91	82,6%	4704	7%	0,389

Table 21. Estimated size values of MR gold nanoparticles using DLS device [all results in nm], the current gold solution was not included in the main project

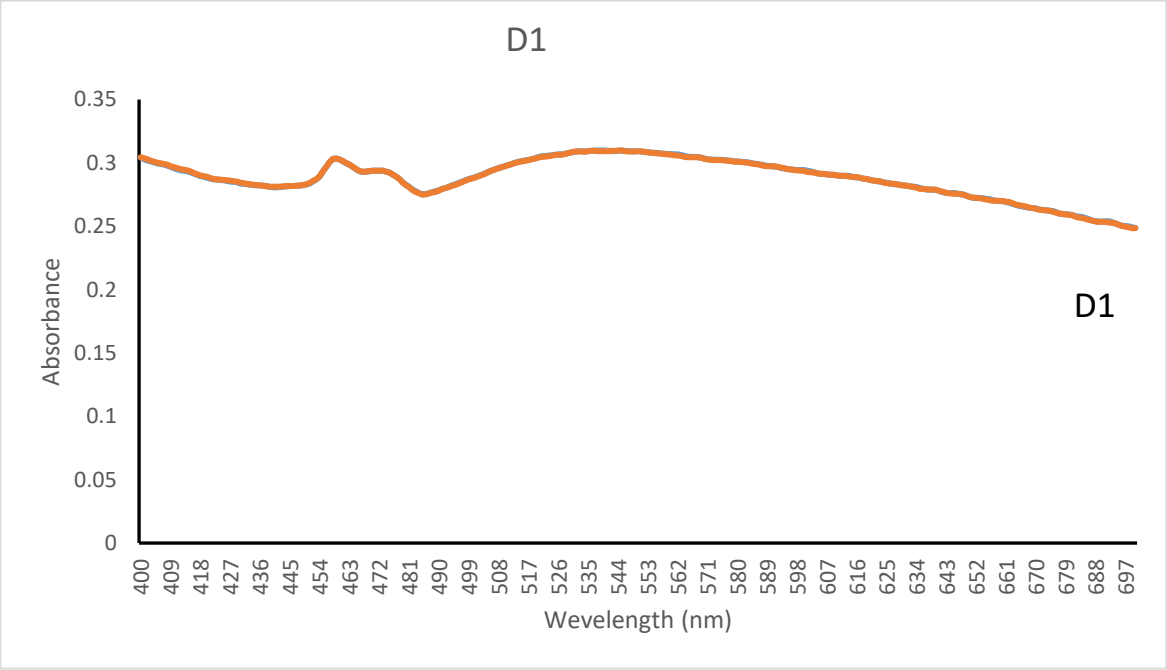

Figure 27. UV-Vis spectrum of MR gold nanoparticles without visible SPR [sample 1]

10.3 Raw data of DLS and UV-Vis measurements

	Measurement 1 (nm)	Measurement 2 (nm)	Measurement 3 (nm)	Average
Undiluted	25.63	25.90	27.52	26.35
AuNP-MR 1:2	25.36	33.40	25.74	28.1
AuNP-MR 1:5	25.24	28.09	23.48	25.6
AuNP-MR 1:10	26.11	33.88	28.39	29.46
AuNP-MR 1:20	25.91	23.29	26.07	25.09
Total average	26.93 nm			

Table 22. Estimated size values of MR gold nanoparticles [sample 2] using DLS device [all results in nm], the current gold solution was not included in the main project

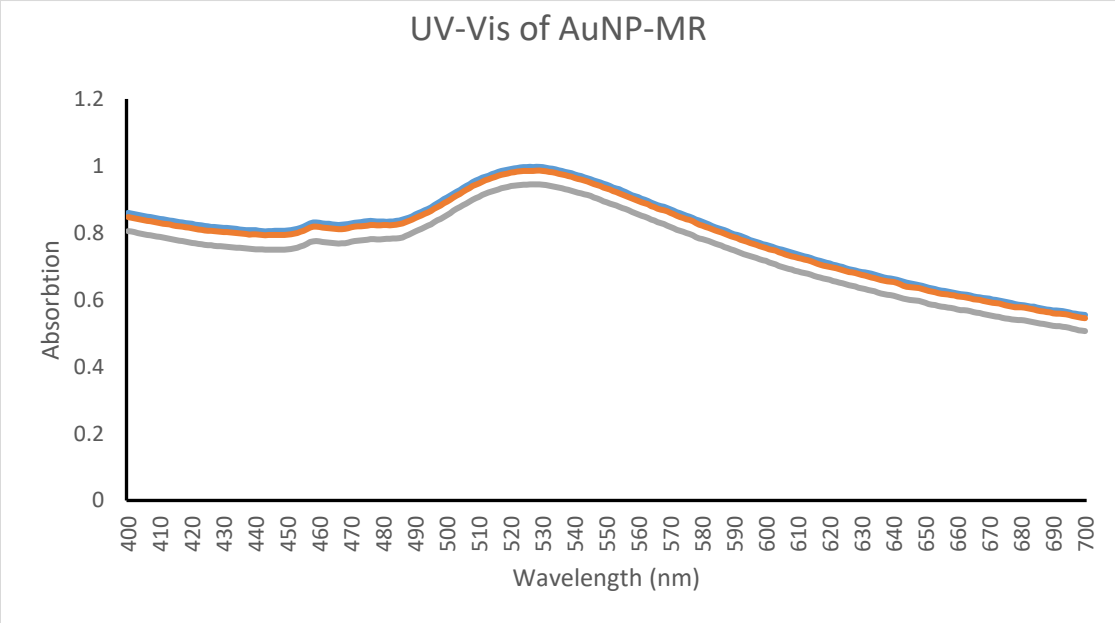

Figure 28. UV-Vis spectrum of MR gold nanoparticles [sample 2] with clearly visible SPR on 529 nm

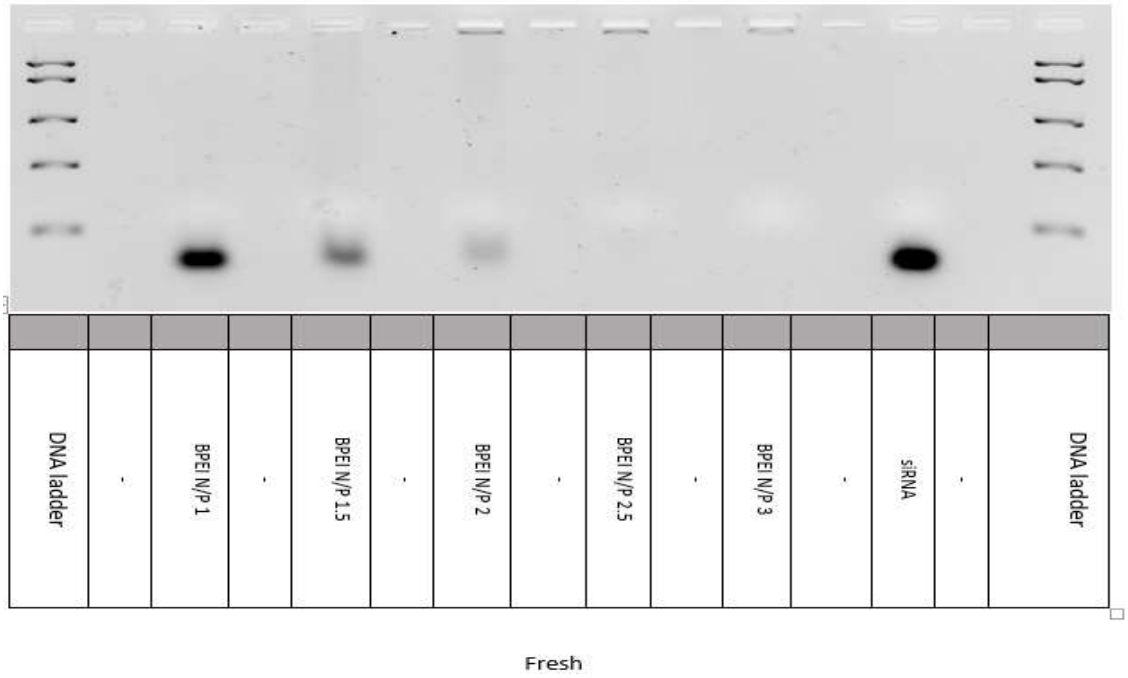

Figure 29. An addition gel as part of polyplexing experiment with lower N/P ratios

11. References

AG, L. I. (2019) *Dynamic Light Scattering*. Available at: https://lsinstruments.ch/en/technology/dynamic-light-scattering-dls (Accessed: 25 September 2019).

Akhtar, S. and Benter, I. F. (2007) 'Nonviral delivery of synthetic siRNAs in vivo', *Journal of Clinical Investigation*. doi: 10.1172/JCI33494.

Amendola, V. *et al.* (2017) 'Surface plasmon resonance in gold nanoparticles: A review', *Journal of Physics Condensed Matter*. doi: 10.1088/1361-648X/aa60f3.

Amendola, V. and Meneghetti, M. (2009) 'Size evaluation of gold nanoparticles by UV-vis spectroscopy', *Journal of Physical Chemistry C*. doi: 10.1021/jp8082425.

Blaese, R. M. *et al.* (1995) 'T lymphocyte-directed gene therapy for ADA-SCID: Initial trial results after 4 years', *Science*. doi: 10.1126/science.270.5235.475.

Boisselier, E. and Astruc, D. (2009) 'Gold nanoparticles in nanomedicine: Preparations, imaging, diagnostics, therapies and toxicity', *Chemical Society Reviews*. doi: 10.1039/b806051g.

C. Martínez, J. *et al.* (2013) 'Alternative Metodology for Gold Nanoparticles Diameter Characterization Using PCA Technique and UV-VIS Spectrophotometry', *Nanoscience and Nanotechnology*. doi: 10.5923/j.nn.20120206.06.

Carthew, R. W. and Sontheimer, E. J. (2009) 'Origins and Mechanisms of miRNAs and siRNAs', *Cell*. doi: 10.1016/j.cell.2009.01.035.

Daniel, M. C. and Astruc, D. (2004) 'Gold Nanoparticles: Assembly, Supramolecular Chemistry, Quantum-Size-Related Properties, and Applications Toward Biology, Catalysis, and Nanotechnology', *Chemical Reviews*. doi: 10.1021/cr030698+.

Decker, S. (2019) *Quantification of LPEI (Copper Assay)*.

Edwards, P. P. and Thomas, J. M. (2007) 'Gold in a metallic divided state - From Faraday to present-day nanoscience', *Angewandte Chemie - International Edition*. doi: 10.1002/anie.200700428.

Filipe, V., Hawe, A. and Jiskoot, W. (2010) 'Critical evaluation of nanoparticle tracking analysis (NTA) by NanoSight for the measurement of nanoparticles and protein aggregates', *Pharmaceutical Research*. doi: 10.1007/s11095-010-0073-2.

Fire, A. *et al.* (1998) 'Potent and specific genetic interference by double-stranded RNA in caenorhabditis elegans', *Nature*. doi: 10.1038/35888.

Frei, M. *et al.* (2012) 'Linker dependent bond rupture force measurements in single-

molecule junctions', *Journal of the American Chemical Society*. doi: 10.1021/ja211590d.

Gao, X., Kim, K. S. and Liu, D. (2007) 'Nonviral gene delivery: What we know and what is next', *AAPS Journal*. doi: 10.1208/aapsj0901009.

von Gersdorff, K. *et al.* (2006) 'The Internalization Route Resulting in Successful Gene Expression Depends on both Cell Line and Polyethylenimine Polyplex Type', *Molecular Therapy*. doi: 10.1016/j.ymthe.2006.07.006.

Giljohann, D. A. *et al.* (2010) 'Gold nanoparticles for biology and medicineGiljohann, D. A., Seferos, D. S., Daniel, W. L., Massich, M. D., Patel, P. C., & Mirkin, C. A. (2010). Gold nanoparticles for biology and medicine. Angewandte Chemie - International Edition. https://doi.org/10.10', *Angewandte Chemie - International Edition*. doi: 10.1002/anie.200904359.

Ginn, S. L. *et al.* (2018) 'Gene therapy clinical trials worldwide to 2017: An update', *Journal of Gene Medicine*. doi: 10.1002/jgm.3015.

GmbH, A. P. (no date) *The principles of dynamic light scattering*. Available at: https://wiki.anton-paar.com/en/the-principles-of-dynamic-light-scattering/ (Accessed: 25 September 2019).

Godfrey, C. *et al.* (2017) 'Delivery is key: lessons learnt from developing splice-switching antisense therapies', *EMBO Molecular Medicine*. doi: 10.15252/emmm.201607199.

Grandbois, M. *et al.* (1999) 'How strong is a covalent bond', *Science*. doi: 10.1126/science.283.5408.1727.

Günther, M. *et al.* (2011) 'Polyethylenimines for RNAi-mediated gene targeting in vivo and siRNA delivery to the lung', *European Journal of Pharmaceutics and Biopharmaceutics*. doi: 10.1016/j.ejpb.2010.11.007.

Hacein-Bey-Abina, Salima *et al.* (2003) 'A Serious Adverse Event after Successful Gene Therapy for X-Linked Severe Combined Immunodeficiency', *New England Journal of Medicine*. doi: 10.1056/nejm200301163480314.

Hacein-Bey-Abina, S. *et al.* (2003) 'LMO2-Associated Clonal T Cell Proliferation in Two Patients after Gene Therapy for SCID-X1', *Science*. doi: 10.1126/science.1088547.

Haiss, W. *et al.* (2015) 'Determination of Size and Concentration of Gold Nanoparticles from UV − Vis Spectra Determination of Size and Concentration of Gold Nanoparticles from UV - Vis Spectra', *Analytical Chemistry*. doi: 10.1021/ac0702084.

Häkkinen, H. (2012) 'The gold-sulfur interface at the nanoscale', *Nature Chemistry*. doi: 10.1038/nchem.1352.

Von Harpe, A. *et al.* (2000) 'Characterization of commercially available and synthesized polyethylenimines for gene delivery', *Journal of Controlled Release*. doi: 10.1016/S0168-3659(00)00317-5.

Havens, M. A. and Hastings, M. L. (2016) 'Splice-switching antisense oligonucleotides as therapeutic drugs', *Nucleic Acids Research*. doi: 10.1093/nar/gkw533.

Hellman, L. M. and Fried, M. G. (2007) 'Electrophoretic mobility shift assay (EMSA) for detecting protein-nucleic acid interactions', *Nature Protocols*. doi: 10.1038/nprot.2007.249.

Helmschrodt, C. *et al.* (2017) 'Polyethylenimine Nanoparticle-Mediated siRNA Delivery to Reduce α-Synuclein Expression in a Model of Parkinson's Disease', *Molecular Therapy - Nucleic Acids*. doi: 10.1016/j.omtn.2017.08.013.

Hickerson, R. P. *et al.* (2008) 'Stability study of unmodified siRNA and relevance to clinical use', *Oligonucleotides*. doi: 10.1089/oli.2008.0149.

Höbel, S. and Aigner, A. (2010) 'Polyethylenimine (PEI)/siRNA-mediated gene knockdown in vitro and in vivo.', *Methods in molecular biology (Clifton, N.J.)*. doi: 10.1007/978-1-60761-588-0_18.

Howe, S. J. *et al.* (2008) 'Insertional mutagenesis combined with acquired somatic mutations causes leukemogenesis following gene therapy of SCID-X1 patients', *Journal of Clinical Investigation*. doi: 10.1172/JCI35798.

Huang, X. and El-Sayed, M. A. (2010) 'Gold nanoparticles: Optical properties and implementations in cancer diagnosis and photothermal therapy', *Journal of Advanced Research*. doi: 10.1016/j.jare.2010.02.002.

Inc., © 2019 Cytodiagnostics (no date) *Gold Nanoparticle Handling and Storage*. Available at: http://www.cytodiagnostics.com/store/pc/viewcontent.asp?idpage=7 (Accessed: 8 October 2019).

Inc., C. (2019) *Introduction to Gold Nanoparticle Characterization*.

Joseph, D. and Geckeler, K. E. (2009) 'Surfactant-directed multiple anisotropic gold nanostructures: Synthesis and surface-enhanced Raman scattering', *Langmuir*. doi: 10.1021/la9019052.

Juliano, R. *et al.* (2008) 'Mechanisms and strategies for effective delivery of antisense and siRNA oligonucleotides', *Nucleic Acids Research*. doi: 10.1093/nar/gkn342.

KGaA, M. (1999) *Ethidium Bromide*. Available at: https://www.sigmaaldrich.com/technical-documents/articles/biology/ethidium-bromide.html.

Khlebtsov, N. G. (2008) 'Determination of size and concentration of gold nanoparticles from extinction spectra', *Analytical Chemistry*. doi: 10.1021/ac800834n.

Krüger, D. *et al.* (2002) 'Pulling Monatomic Gold Wires with Single Molecules: An Ab

Initio Simulation', *Physical Review Letters*. doi: 10.1103/PhysRevLett.89.186402.

Lee, S. H. *et al.* (2008) 'Amine-functionalized gold nanoparticles as non-cytotoxic and efficient intracellular siRNA delivery carriers', *International Journal of Pharmaceutics*. doi: 10.1016/j.ijpharm.2008.07.027.

Lewinski, N., Colvin, V. and Drezek, R. (2008) 'Cytotoxicity of nanopartides', *Small*. doi: 10.1002/smll.200700595.

Liu, D., Wang, Z. and Jiang, X. (2011) 'Gold nanoparticles for the colorimetric and fluorescent detection of ions and small organic molecules', *Nanoscale*. doi: 10.1039/c0nr00887g.

Ltd., N. (2013) *NanoSight NTA 2.3 Analytical Software Operation Manual*. Amesbury, Wiltshire, UK.

Ltd, M. I. (no date) *Dynamic Light Scattering: An Introduction in 30 Minutes*. Available at: https://warwick.ac.uk/fac/cross_fac/sciencecity/programmes/internal/themes/am2/booking/particlesize/intro_to_dls.pdf (Accessed: 26 September 2019).

Maria Dusinska, Zuzana Magdolenova (auth.), Manfred Ogris, D. O. (eds. . (2013) *Nanotechnology for Nucleic Acid Delivery: Methods and Protocols*. Humana Press.

McClorey, G. and Wood, M. J. (2015) 'An overview of the clinical application of antisense oligonucleotides for RNA-targeting therapies', *Current Opinion in Pharmacology*. doi: 10.1016/j.coph.2015.07.005.

Murray, C. B., Kagan, C. R. and Bawendi, M. G. (2000) 'Synthesis and characterization of monodisperse nanocrystals and close-packed nanocrystal assemblies', *Annual Review of Materials Science*. doi: 10.1146/annurev.matsci.30.1.545.

nanoComposix (2019) *Spectroscopic Analysis (UV-Visible Spectroscopy)*. Available at: https://nanocomposix.com/pages/characterization-techniques#spectroscopic-analysis.

NanoSight Ltd., Minton Park, Amesbury, Wiltshire SP4 7RT, U. (2012) *NanoSight NTA 2.3 Analytical Software*, *P554I*. Available at: https://sydney.edu.au/medicine/bosch/facilities/molecular-biology/P554I NTA 2_3 Manual.pdf.

NanoSight NS500 (no date). Available at: https://www.malvernpanalytical.com/en/support/product-support/nanosight-range/nanosight-ns500 (Accessed: 25 September 2019).

Neu, M., Fischer, D. and Kissel, T. (2005) 'Recent advances in rational gene transfer vector design based on poly(ethylene imine) and its derivatives', *Journal of Gene Medicine*. doi: 10.1002/jgm.773.

Ozcan, G. *et al.* (2015) 'Preclinical and clinical development of siRNA-based therapeutics', *Advanced Drug Delivery Reviews*. doi: 10.1016/j.addr.2015.01.007.

Park, S.-H. and Raines, R. T. (2008) 'Green fluorescent protein as a signal for protein-protein interactions', *Protein Science*. doi: 10.1002/pro.5560061107.

Peng, H. *et al.* (2016) 'Sustained delivery of siRNA/PEI complex from in situ forming hydrogels potently inhibits the proliferation of gastric cancer', *Journal of Experimental and Clinical Cancer Research*. doi: 10.1186/s13046-016-0334-y.

Qian, H., Sheetz, M. P. and Elson, E. L. (1991) 'Single particle tracking. Analysis of diffusion and flow in two-dimensional systems', *Biophysical Journal*. doi: 10.1016/S0006-3495(91)82125-7.

Rahman, S. (2016) 'Size and Concentration Analysis of Gold Nanoparticles With Ultraviolet-Visible Spectroscopy', *Undergraduate Journal of Mathematical Modeling: One + Two*. doi: 10.5038/2326-3652.7.1.4872.

Sakho, E. H. M. *et al.* (2017) 'Dynamic Light Scattering (DLS)', in *Thermal and Rheological Measurement Techniques for Nanomaterials Characterization*. doi: 10.1016/B978-0-323-46139-9.00002-5.

Saveyn, H. *et al.* (2010) 'Accurate particle size distribution determination by nanoparticle tracking analysis based on 2-D Brownian dynamics simulation', *Journal of Colloid and Interface Science*. doi: 10.1016/j.jcis.2010.09.006.

Schützhofer, A. (2018) *Biophysical Characterization of Quantoplexes: Potential Bioimaging Applications*. University of Vienna.

Sharma, V. K., Rungta, P. and Prasad, A. K. (2014) 'Nucleic acid therapeutics: Basic concepts and recent developments', *RSC Advances*. doi: 10.1039/c3ra47841f.

Shukla, R. *et al.* (2005) 'Biocompatibility of gold nanoparticles and their endocytotic fate inside the cellular compartment: A microscopic overview', *Langmuir*. doi: 10.1021/la0513712.

Sigmon, J. and Larcom, L. L. (1996) 'The effect of ethidium bromide on mobility of DNA fragments in agarose gel electrophoresis', *Electrophoresis*. doi: 10.1002/elps.1150171003.

Skulason, H. and Frisbie, C. D. (2000) 'Detection of discrete interactions upon rupture of Au microcontacts to self-assembled monolayers terminated with -S(CO)CH3 or -SH', *Journal of the American Chemical Society*. doi: 10.1021/ja994524e.

Somia, N. and Verma, I. M. (2000) 'Gene therapy: Trials and tribulations', *Nature Reviews Genetics*, 1(2), pp. 91–99. doi: 10.1038/35038533.

Sridharan, K. and Gogtay, N. J. (2016) 'Therapeutic nucleic acids: current clinical status', *British Journal of Clinical Pharmacology*. doi: 10.1111/bcp.12987.

Turkevich, J., Stevenson, P. C. and Hillier, J. (1951) 'A study of the nucleation and growth processes in the synthesis of colloidal gold', *Discussions of the Faraday Society*. doi: 10.1039/DF9511100055.

Ungaro, F. *et al.* (2003) 'Spectrophotometric determination of polyethylenimine in the presence of an oligonucleotide for the characterization of controlled release formulations', *Journal of Pharmaceutical and Biomedical Analysis*. doi: 10.1016/S0731-7085(02)00571-X.

Uskoković, V. *et al.* (2011) 'Dynamic light scattering and zeta potential of colloidal mixtures of amelogenin and hydroxyapatite in calcium and phosphate rich ionic milieus', *Archives of Oral Biology*. doi: 10.1016/j.archoralbio.2010.11.011.

Vanegas, J. P., Scaiano, J. C. and Lanterna, A. E. (2017) 'Thiol-Stabilized Gold Nanoparticles: New Ways to Displace Thiol Layers Using Yttrium or Lanthanide Chlorides', *Langmuir*. doi: 10.1021/acs.langmuir.7b01898.

Wang, X. *et al.* (2015) 'Polyethylenimine mediated magnetic nanoparticles for combined intracellular imaging, siRNA delivery and anti-tumor therapy', *RSC Advances*. doi: 10.1039/c5ra18464a.

Watts, J. and Corey, D. (2012) 'Gene silencing by siRNAs and antisense oligonucleotides in the laboratory and the clinic', *The Journal of pathology*. doi: 10.1002/path.2993.Gene.

Wen, T. *et al.* (2017) 'A facile, sensitive, and rapid spectrophotometric method for copper(II) ion detection in aqueous media using polyethyleneimine', *Arabian Journal of Chemistry*. doi: 10.1016/j.arabjc.2013.06.013.

Wikimedia Foundation, I. (2019) *Electrophoretic mobility shift assay*. Available at: https://en.wikipedia.org/wiki/Electrophoretic_mobility_shift_assay (Accessed: 4 October 2019).

Wikimedia Foundation, I. (no date) *Dynamic light scattering*. Available at: https://en.wikipedia.org/wiki/Dynamic_light_scattering (Accessed: 25 September 2019).

Wikipedia contributors (no date) *Nanoparticle tracking analysis*. Available at: https://en.wikipedia.org/wiki/Nanoparticle_tracking_analysis (Accessed: 26 September 2019).

Xue, Y. *et al.* (2014) 'Quantifying thiol-gold interactions towards the efficient strength control', *Nature Communications*. doi: 10.1038/ncomms5348.

Yokoo, T. *et al.* (2018) 'Nucleic Acid-Based Therapy: Development of a Nonviral-Based Delivery Approach', in. doi: 10.5772/intechopen.80741.